

RESEARCH

Open Access



# Bradykinesia and postural instability in a model of prodromal synucleinopathy with $\alpha$ -synuclein aggregation initiated in the gigantocellular nuclei

Vasileios Theologidis<sup>1,4</sup>, Sara A. Ferreira<sup>2</sup>, Nanna M. Jensen<sup>3</sup>, Diana Gomes Moreira<sup>1</sup>, Ole A. Ahlgreen<sup>2</sup>, Mads W. Hansen<sup>2</sup>, Emilie D. Rosenberg<sup>2</sup>, Mette Richner<sup>2</sup>, Islam Faress<sup>3</sup>, Hjalte Gram<sup>3</sup>, Poul Henning Jensen<sup>3</sup>, Per Borghammer<sup>1</sup>, Jens R. Nyengaard<sup>1,4,5</sup>, Marina Romero-Ramos<sup>2</sup>, Christian B. Vægter<sup>2</sup>, Wilma D. J. van de Berg<sup>6</sup>, Nathalie Van Den Berge<sup>1,4</sup> and Asad Jan<sup>7\*</sup> 

## Abstract

$\alpha$ -Synuclein (aSyn) accumulation within the extra-nigral neuronal populations in the brainstem, including the gigantocellular nuclei (GRN/Gi) of reticular formation, is a recognized feature during the prodromal phase of Parkinson disease (PD). Accordingly, there is a burgeoning interest in animal model development for understanding the pathological significance of extra-nigral synucleinopathy, in relation to motor and/or non-motor symptomatology in PD. Here, we report an experimental paradigm for the induction of aSyn aggregation in brainstem, with stereotaxic delivery of pre-formed fibrillar (PFF) aSyn in the pontine GRN of transgenic mice expressing the mutant human Ala53Thr aSyn (M83 line). Our data show that PFF aSyn-induced aggregate pathology in GRN and distinct nuclei of subcortical motor system leads to progressive decline in home cage activity, which was accompanied by postural instability and impaired motor coordination. The progressive accumulation of aSyn pathology in brainstem and motor neurons in lumbar spinal cord heralded the onset of a moribund stage, which culminated in impaired survival. Collectively, our observations suggest an experimental framework for studying the pathological significance of aSyn aggregation in GRN in relation to features of movement disability in PD. With further refinements, we anticipate that this model holds promise as a test-bed for translational research in PD and related disorders.

**Keywords** Parkinson disease, Alpha-synuclein, Lewy pathology, Gigantocellular nucleus

\*Correspondence:

Asad Jan

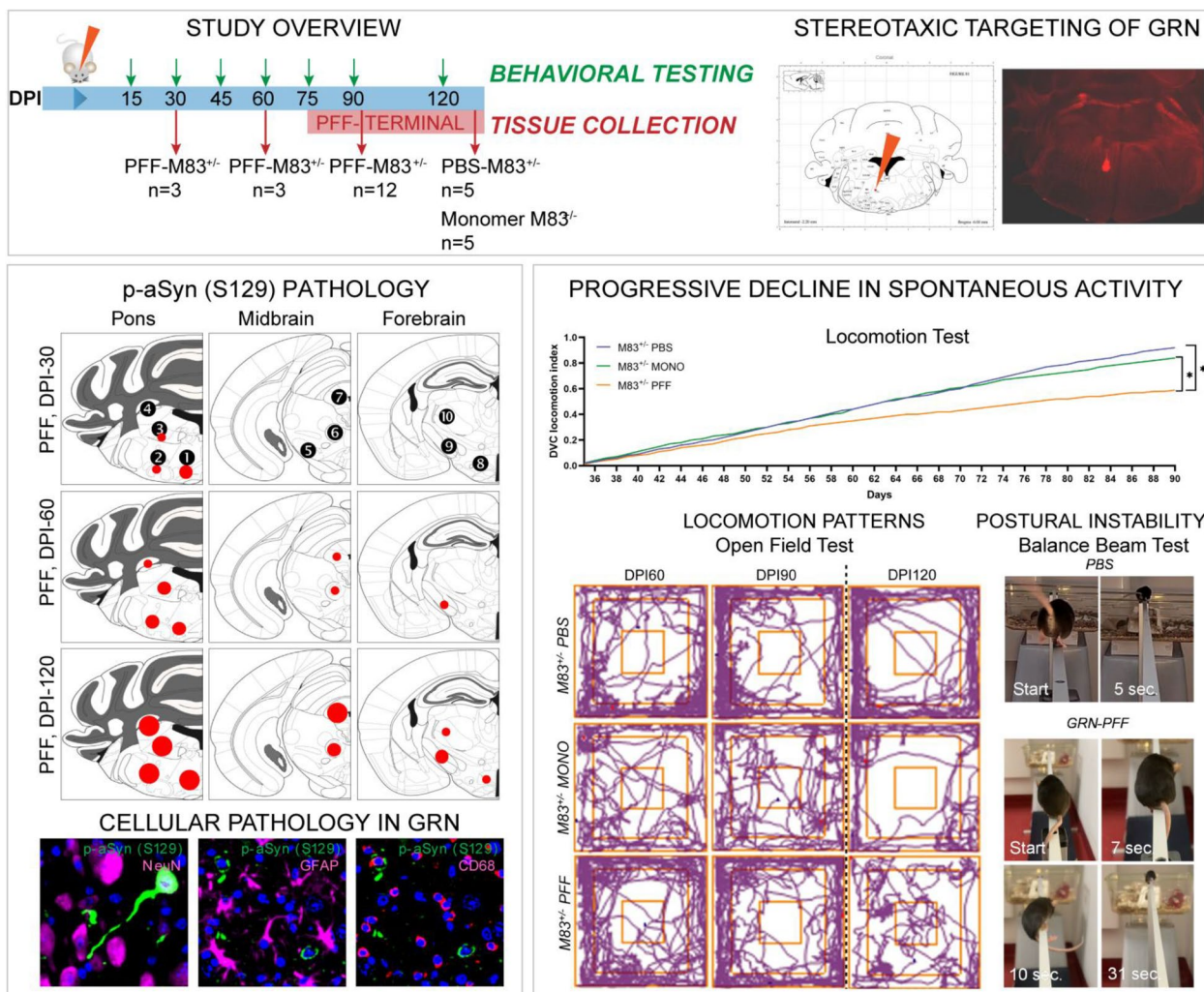
[ajan@aiaas.au.dk](mailto:ajan@aiaas.au.dk)

Full list of author information is available at the end of the article



© The Author(s) 2025. **Open Access** This article is licensed under a Creative Commons Attribution-NonCommercial-NoDerivatives 4.0 International License, which permits any non-commercial use, sharing, distribution and reproduction in any medium or format, as long as you give appropriate credit to the original author(s) and the source, provide a link to the Creative Commons licence, and indicate if you modified the licensed material. You do not have permission under this licence to share adapted material derived from this article or parts of it. The images or other third party material in this article are included in the article's Creative Commons licence, unless indicated otherwise in a credit line to the material. If material is not included in the article's Creative Commons licence and your intended use is not permitted by statutory regulation or exceeds the permitted use, you will need to obtain permission directly from the copyright holder. To view a copy of this licence, visit <http://creativecommons.org/licenses/by-nc-nd/4.0/>.

**Graphical abstract**



**Introduction**

Idiopathic Parkinson disease (PD) is the most common cause of movement disability, clinically defined by the acronym TRAP: resting Tremor, Rigidity, difficulty in movement initiation (bradykinesia/Akinesia), and Postural instability [36, 52]. The prevalent notion concerning the movement disability in PD implicates the progressive decline of dopaminergic neurotransmission in the nigro-striatal circuitry, arising due to the loss of dopaminergic neurons in the midbrain substantia nigra-*pars compacta* (SNpc) [36, 52]. In addition, a substantial number of PD patients report non-motor symptoms (olfaction, autonomic, sleep and pain-related), which significantly impair the quality of life [57]. In a larger context, it is increasingly being recognized that the nigro-centric view is not

sufficient to account for the heterogeneity in the clinical presentation of PD and related disorders [33, 52, 57]. The nature of pathological process(es) which trigger neuronal dysfunction and/or neurodegeneration in SNpc remains an active subject of investigation. In this regard, aggregation of  $\alpha$ -Synuclein (aSyn; gene symbol *SNCA*) in SNpc and several extra-nigral regions (i.e. outside SNpc) is considered to be a potent aggravating factor in the pathogenesis of PD and related synucleinopathies [19, 31].

According to the Braak staging scheme, neuronal populations within the dorsal motor nucleus of the vagus nerve (*dmX*), locus coeruleus (LC) and the nuclei of reticular formation including the gigantocellular nuclei (GRN/Gi) bear the brunt of cellular aSyn pathology during the early stages of PD [7–9, 34, 58]. These

observations ushered novel efforts in the development of refined animal models for studying the neurological basis of PD symptomatology, which are not confined by the prevalent nigro-centric view. The utility of these efforts is highlighted by the studies showing that extra-nigral brainstem synucleinopathy (e.g. in *dmX* and/or LC) recapitulates PD-like non-motor symptoms and autonomic dysfunction in rodents [10, 38, 49, 65]. Intriguingly, the significance of cellular aSyn pathology affecting GRN and nearby nuclei of brainstem reticular formation in the context of PD symptomatology remains largely unexplored.

The GRN is a prominent collection of neurons within the paramedian parts of pontomedullary reticular formation [32]. It has been suggested that neuronal populations of GRN, in concert with basal ganglia, are involved in smooth execution of complex movements, including turning, gait stance and stopping the locomotion in freely moving animals [16, 17, 42]. Neuroanatomically, the GRN is one of the major sources of input into the reticulospinal tracts, which converge on motor and premotor neurons at all levels of spinal cord, and modulates the excitability of the spinal motor system [9, 13, 43]. Moreover, in concert with raphe magnus and periaqueductal grey (PAG), the neurons in GRN plausibly modulate pain perception, through descending projections onto the spinal nociceptors in the dorsal horn [26, 32, 47, 68]. In addition, these nuclei also receive substantial input from cerebellum and spinal cord, and are integral components in the coordination of reflex motor activity in the maintenance of posture and balance [9, 32, 67].

Therefore, we hypothesized that direct induction of aSyn aggregation within GRN of rodents will lead to the emergence of unique sensorimotor phenotypes, which could potentially be relevant to PD symptomatology. In particular, we wanted to study the patterns of locomotion, movement coordination and nociception in relation to the emergence and propagation of aSyn pathology in brainstem, with GRN as the initial nidus of aSyn aggregation. In transgenic mice expressing the human mutant Ala53Thr aSyn (M83 line, [29]), we induced de novo aggregation of aSyn in the GRN and neighboring nuclei of subcortical motor system by stereotaxic delivery of pre-formed fibrillar (PFF) aSyn. Our data show that this experimental approach in the rodent model led to progressive motor disability characterized by reduced spontaneous locomotion in home cage and subtle defects in postural motor coordination, long before phenotypes reflecting motor weakness were manifest. With the progression of aSyn pathology into additional nuclei in the brainstem, the animals exhibited worsening deficits in movement coordination and decline in survival. With this context, we highlight the implications of our findings *vis-a-vis* further refinements in model development for

PD and related disorders, and also discuss the limitations of the model.

## Materials and methods

### Generation and characterization of mouse aSyn fibrils

Mouse aSyn fibrils were prepared and characterized in vitro, essentially as described [23, 62]. Briefly, full length recombinant (wild type) mouse aSyn was expressed in BL21(DE3) competent cells and purified using ion-exchange on POROS HQ 50 ion exchange chromatography with a continuous gradient of 0–100% 2 M NaCl in 20 mM Tris pH 6.5. In order to ensure that residual contaminants (e.g. endotoxins, nucleotides and lipids bound to aSyn) were completely removed, the sample was further purified by reverse phase chromatography using a C18 column. The removal of endotoxins (lipoglycans) from the sample was also confirmed by the Pierce™ Chromogenic Endotoxin Quant Kit, ThermoScientific™ (<0.5 EU/mg aSyn). The purified protein was dialyzed in 20 mM ammonium bicarbonate, lyophilized, and stored at –20 °C. The purified aSyn was re-suspended in phosphate-buffered saline (PBS, pH 7.4) at 1 mg/mL and passed through a 100 kDa filter. The monomeric (non-aggregated) aSyn was then incubated with sonicated mouse PFF (5% by mass in PBS) in a seeded aggregation assay [62]. The sample was incubated at 37 °C with continuous shaking at 1050 r.p.m. in a tabletop microtubes shaker (Eppendorf) for 72 h. The insoluble PFF were collected by centrifugation (15,600 g at 25 °C for 30 min) and then re-suspended in PBS. Protein concentration was determined by the BCA assay (Pierce) and a stock solution consisting of 5 mg/mL protein was prepared (in PBS). Subsequently, PFF were sonicated for 20 min using a Branson 250 Sonifier at 30% intensity, and then aliquoted and frozen at –80 °C until further use.

### Animal studies

**Animal care and husbandry.** Transgenic M83 mice [B6;C3-Tg(*Prnp*-SNCA\**A53T*)83Vle/]- [29] were housed at the Skou animal facility at Aarhus University in accordance with Danish regulations and the European Communities Council Directive for laboratory animals. Ethical approval for the mouse colonies (housing, breeding) and the experimental procedures was obtained by Danish authorities Dyreforsøgstilsynet, Denmark (license # 2022–15-0201–01294 issued to CBV, co-author). The animals were housed under a 12 h light/dark cycle and fed with regular chow diet ad libitum. For the study, adult mice (12–14 weeks of age) were used, and the cohorts included both male and female animals.

**Intracerebral aSyn injection in the pontine GRN.** PFF aSyn, monomeric aSyn or PBS were bilaterally delivered into the pontine GRN under isoflurane anesthesia (2–5%),

using the stereotaxic coordinates: [AP (y): -6; ML (x): 0.5 relative to bregma; DV (z)- 2 locations: -5 mm (1  $\mu$ l) and -5.2 mm (1  $\mu$ l) relative to dura]. Hence, 2  $\mu$ l of aSyn preparations (PFF or monomeric, amounting to 10  $\mu$ g total protein) were injected bilaterally, at a flow rate of 0.2  $\mu$ l/min through a 5  $\mu$ l Hamilton syringe (33-gauge needle), connected to a stereotaxic frame. The needle was left in place (at DV -5.2 mm) for an additional 1 min, and then gently withdrawn over 15 s. The main study consisted of the following cohorts of heterozygous M83<sup>+/-</sup> mice: i) PFF aSyn (n=18; 9 males, 9 females), ii) monomeric (non-aggregated) aSyn (n=5; 3 males, 2 females) and iii) PBS (n=5; 3 males, 2 females). As a proof-of-concept, a small pilot study involving stereotaxic delivery of PFF aSyn in GRN of homozygous M83<sup>+/+</sup> mice (n=4; 3 males, 1 female) was also performed using identical experimental setup. After the surgical procedure, the animals were allowed to recover in their home cage (placed on a heated blanket), and received appropriate analgesia based on the veterinarian's recommendations.

### Behavioral assessments

After recovery (14 days), the animals were tested in a battery of sensorimotor tasks (described below) periodically over a period of 120 days post-injection (DPI). Unless indicated otherwise, the animals were acclimatized to the testing environment with standard lighting conditions and ambient background noise for 1 h prior to the tests.

### General locomotion

*Non-invasive monitoring of spontaneous activity in home cage.* Patterns of locomotion and spontaneous activity were monitored in home cage through specialized digitally ventilated cages (DVC) platform (Tecniplast, Italy). This platform is based on the electrical capacitance sensing technology, which incorporates a sensor board equipped with an integrated circuit comprised of 12 electrodes directly beneath the floor of home cage [51]. The DVC circuit measures changes in the electrical capacitance signal from each electrode in response to the movement of a water-filled body (animal) close to or away from a given electrode. The measurements, performed approximately 4 times per second, are remotely relayed to the centralized DVC analytics platform (Tecniplast, Italy). In this web-based interface, time-stamped data for each cage can be visualized using in-built tools (e.g. daily rhythms, cumulative activity/locomotion index aggregated per minute/hour, bedding status, light or dark period activity, heatmaps etc.). In the default setup, the DVC analytics web-interface plots the animal locomotion index as arbitrary units normalized between 0 and 100%, representing the overall activity performed in the cage by the animals, i.e., the signal is measured for each cage and

not each animal, unless the animals are singly housed. The detailed description of DVC working principle and DVC analytics platform is included in the Supplementary Information.

*Open-Field Test.* General locomotor activity and exploratory behavior were assessed in an open-field chamber (40 cm  $\times$  40 cm  $\times$  30 cm) with video recordings over a period of 10 min obtained through an overhead USB camera, operated by the ANY-maze analytical software (Vendor: Stoelting Europe). The test parameters included distance traveled (m), mean speed (m/s), time freezing (s), and number of entries into defined zones (center, periphery and intermediate).

### Balance, movement coordination and motor strength

*Balance beam Test.* Fine motor coordination and balance were assessed by the balance beam test with slight modifications [45]. The test apparatus consisted of flat surface metal beams (length: 1 m; width: 8 cm or 16 cm), supported by two poles (height: 60 cm), and equipped with a nylon hammock underneath (10 cm above the ground). A source of bright light (lamp) was used as an aversive stimulus on the starting end. The mice were trained to traverse the 2 beams (3 attempts on 2 consecutive days; each attempt separated by 15 min), towards a clean cage with some bedding from the home cage. During the test, video recordings of the behavior were obtained through a USB camera (operated by Microsoft Windows), placed within 5 cm from the starting end and at the same height as the beam. Each animal was tested 2 times on each beam with inter-trial duration of 15–20 min, and the mean of the measurements was calculated. Video recordings in slow motion were analyzed for the traversal time (s), number of hindpaw slips and mean speed of traversal (m/s).

*Pole Test.* Fine motor coordination was assessed in a pole test [30], with a test apparatus consisting of a wooden pole (height: 50 cm, diameter: 1 cm), which was supported by a circular base stand (diameter: 10 cm) placed in a clean cage containing some bedding from the home cage. The mice were gently placed within 2 cm of the top of the pole facing up and away from the testing personnel. Video recordings of the behavior were obtained through a USB camera (operated by Microsoft Windows), placed within 25 cm from the pole such that the whole length of pole could be recorded (from a side view, approx. 90°). Each animal was trained over 2 consecutive days with 5 trials, with inter-trial duration of 15 min. During the test, each animal was subjected to 3 trials, with inter-trial duration of 15–20 min, and the average of the measurements was calculated. Video recordings in slow motion were analyzed for assessing the turning time (t1), traversal time after turning and reaching the base stand (t2) and total time on the pole

( $t_1 + t_2$ ). If the animal paused while descending, the trial was repeated. If the animal fell off during the descent, a maximum score of 25 s was assigned to the traversal time ( $t_2$ ) and 30 s to the total time ( $t_1 + t_2$ ).

**Rotarod Test.** Fore- and hindlimb motor coordination and balance were assessed by placing the mice on an accelerating rod (Rotarod; LE8500 Harvard Apparatus)-[11]. The mice were trained to walk in a forward direction on the rotarod for 60–90 s with a fixed rotation rate of 4 rpm (3 attempts on 3 consecutive days; each attempt separated by 10 min). If the animal fell off before 60 s, it was returned to home cage and the training attempt was resumed after approx. 15 min. During the test, the animal was placed on the rotarod and acceleration from 4 to 40 rpm in 120 s was initiated. Each animal was tested 3 times, with inter-trial duration of 15–20 min, and the average of the measurements was calculated. The analyses included time (latency in seconds) to fall and speed at fall (r.p.m.).

**Grip strength Test.** Limb motor strength was assessed by a grip strength test apparatus (BIOSEB, BIO-GS4), according to the manufacturer's instructions. During the test, the mice were held by the tail and lowered onto a horizontal metal grid connected to a sensor detecting peak tension. After the animal grabbed the metal grid, it was pulled backwards by the tail in horizontal plane with a gentle constant pressure. The average maximal peak force (grams) exerted by the paws was recorded from 3 consecutive trials, with an inter-trial interval of approx. 10 s.

**Footprint Test.** Gait stance was assessed by a footprint test with slight modifications [11]. The apparatus consisted of a flat wooden platform (length: 50 cm, width: 5 cm) supported on each end by two wooden poles attached underneath (height: approx. 10 cm). The forepaws and the hindpaws were coated with red and black nontoxic paint, respectively. The mice were placed on a cut sheet of white paper (length: 40 cm, width: 5 cm) lightly affixed to the platform, and trained to traverse the platform to a clean cage with some bedding material from home cage. The training consisted of 3 consecutive attempts on 2 consecutive days (each attempt separated by 2–3 min) one day prior to the test (except, the pre-terminal stage; see Results). A fresh sheet of paper was placed for each mouse during each training session.

On the testing day, the mice were allowed to traverse the platform with a fresh sheet of paper and the paint was air-dried for 30 min. Then, the footprint patterns were analyzed for measures of gait stance from 2 to 3 consecutive steps made in the forward direction, excluding footprints made at the beginning and end of the platform. The measures (all in cm) include: (1) Stride length: average distance of forward movement between each

stride. (2) Step width: average diagonal distance between alternating front and rear paws. (3) Rear base of support (RBOS) and (4) Frontal base of support (FBOS): average distance between left and right footprints (rear or front paws, respectively), represented by a perpendicular line connecting the center of a given footstep to its opposite preceding and proceeding steps. (5) Step alternation: Overlap between left or right footprints in consecutive steps, i.e. distance between the center of the hind footprint and the center of the preceding front footprint. For the gait stance parameters, the mean value of each set comprising 2–3 values in each measure was used in the subsequent analyses.

**Hindlimb Clasping Test.** Assessment of hindlimb clasping was performed by a modified tail suspension test [24, 69]. Freely moving, non-anesthetized, mice were held by the tail and lifted in air for 10 s. Severity of clasping was scored on a scale of 0–3, as follows: a) *Score 0, No clasping* (both hindlimbs were consistently splayed outwards, and away from the abdomen for more than 50% of the time suspended); b) *Score 1, Mild clasping* (one hindlimb was retracted toward the abdomen for more than 50% of the time suspended); c) *Score 2, Moderate clasping* (both hindlimbs were partially retracted toward the abdomen for more than 50% of the time suspended); and d) *Score 3, Severe clasping* (both hindlimbs were entirely retracted, and touching the abdomen for more than 50% of the time suspended).

## Nociception

**Hot plate.** Thermal nociception/allodynia was assessed using a hot plate apparatus (VWR), preheated to a stable temperature of  $55\text{ }^{\circ}\text{C} \pm 0.5$  [63]. For the test, a bottomless plexiglass chamber (15 cm  $\times$  15 cm  $\times$  15 cm) was placed on a flat metal surface and the animals were individually lowered into the chamber. The latency to response (sec) was recorded manually, when the animal licked the paws or jumped. A cut-off maximum time (30 s) was used and animals were immediately removed after the response in the test.

**Von Frey.** Mechanical allodynia was assessed by manually applying the calibrated Semmes–Weinstein monofilaments (Stoelting) of ascending force (0.16–2.00 g) onto the plantar surface of the hindpaws, avoiding food pads [53]. During the test, the animals were acclimatized in a plexiglas container placed over a mesh metal grid for approximately 10 min prior to testing in an ambient lit room and quiet surroundings. A positive response to given filament application was characterized by sudden paw withdrawal, paw licking or jerky flailing of toes. Each filament was applied 5 times for maximum duration of 5 s to the test subject. The threshold response (g) to a

given filament was recorded at a positive response to at least three out of 5 applications of the same filament.

## Histological analyses

### Human studies

#### *Study cohort, ethics approval and consent, and pathological assessment*

Post-mortem brain tissue from subjects with clinical parkinsonism and neurologically normal controls were acquired from the Netherlands Brain Bank (NBB; Amsterdam, The Netherlands, <http://brainbank.nl>). Donors or their next of kin signed informed consent for brain autopsy, the use of brain tissue and the use of medical records for research purposes. The brain donor program of the NBB and NABCA is approved by the local medical ethics committee of the VUmc, Amsterdam (approval# NBB 2009.148). Demographic features and clinical symptoms were retrieved from the clinical files, including sex, age at symptom onset, age at death, disease duration, presence of dementia and parkinsonism. Braak stages for aSyn pathology were determined using the BrainNet Europe (BNE) criteria. Braak neurofibrillary stages were determined according to the NIA-AA consensus criteria. A summary of the clinical and pathological characteristics for all cases can be found in the supplementary file (Table S1).

#### *Human tissue processing and immunohistochemistry (IHC) analyses*

IHC detection of p-aSyn (S129) was performed on 6  $\mu$ m thick formalin-fixed paraffin-embedded (FFPE) tissue sections of medulla oblongata, following deparaffinization and blocking of endogenous peroxidase, according to previously established methods [66]. Nonspecific binding was blocked by incubating the sections in Tris-Buffered Saline (TBS) containing 3% normal donkey serum for 30 min at room temperature (RT). Then, the sections were incubated (overnight, at 4 °C) with the primary antibody for detecting p-S129 aSyn (rabbit mAb EP1536Y Abcam, #ab51253- 1:4000). Then, the sections were stained with secondary detection solution Envision anti-rabbit (DAKO cat# K4003) for 30 min at RT. Color was developed using the DAB (3,3'-diaminobenzidine) chromogen for 10 min at RT. Nuclear counterstaining was performed in hematoxylin for 20 s, after which sections were washed under running tap water for 5 min. Sequential dehydration in ethanol was performed in series: 1×2 min 70%, 1×2 min 80%, 2×2 min 96%, 2×2 min 100%, followed by 3×2 min xylene. Entellan (Merck, cat# 107,960) was used as mounting medium for cover-slipping. After cover-slipping, sections were left to dry overnight in the fume hood. Whole slide digital scans of the immunostained sections were obtained using the

brightfield mode in Olympus VS200 upright microscope at UMC Amsterdam (20X magnification). Slide scans from PD and control cases were imported in QuPath (v. 0.5.1) and p-aSyn (S129) immunopositivity was computed using a pixel classifier on the DAB channel [6]. The data were normalized to the area of the region of interest (ROI) covering GRN.

### Animal studies

*IHC and immunofluorescence (IF) analyses of the mouse brain and lumbar spinal cord sections.* IHC or IF on 10  $\mu$ m thick sections from FFPE tissue was performed after deparaffinization and antigen retrieval in citrate buffer pH 6.0, essentially as described [24]. Nonspecific binding was blocked by incubating the sections in 5% normal donkey serum in TBS (1 h, RT). Then, the sections were incubated (overnight, at 4 °C) with the following primary antibodies (also indicated in the relevant figure legends): phospho-S129 aSyn antibodies (rabbit mAb EP1536Y Abcam, #ab51253- 1:400; rabbit mAb D1R1R, Cell Signaling #23,706- 1:400), Neuronal nuclei marker (NeuN, mouse mAb A60, Millipore #MAB377- 1:1000), astroglial marker, glial fibrillary acidic protein (GFAP, chicken polyclonal, Abcam #4674- 1:200), phagocyte marker CD68 (LAMP4, rat mAb FA-11, Novus Biologicals #NBP2-33,337- 1:200), and Sequestosome 1/p62 (guinea pig, Nordic Biosite GP62-C- 1:200). For double IF co-detection, fluorophore conjugated secondary antibodies were used (Thermo Fisher: AlexaFluor488, AlexaFluor568, AlexaFluor647, 1:1000). For IHC, DAB chromogen detection was performed following prior incubation with biotin conjugated secondary antibody (anti-mouse, Sigma #B7264- 1:100) and Extra-Avidin peroxidase (Sigma #E2886- 1:200). In the lumbar spinal cord samples, co-detection of phospho-S129 aSyn (rabbit mAb EP1536Y Abcam, #ab51253- 1:400; DAB chromogen) and NeuN (mouse mAb A60, Millipore #MAB377- 1:1000; Vina Green chromogen, Biocare Medical #SKU: BRR807A) was performed. Sections were counterstained with hematoxylin (Vector Labs, #H-3401).

For the image analyses, whole slide digital scans of the brain sections were obtained using the Olympus VS120 upright microscope (at AU) equipped for brightfield scanning and fluorescence single-band emitters for DAPI, FITC, Cy3 and Cy5. High resolution IF views were exported using QuPath (v. 0.5.1), for further analysis with ImageJ. ROI for neurons (NeuN+) or microglia (CD68+) were identified using Cellpose [61], followed by manual corrections to determine cell profile numbers expressed as cell profiles/area in mm<sup>2</sup>. NeuN masks defined the neuronal area in each tissue section. P-aSyn (S129) and GFAP area fractions were defined by thresholding at the same level across all sections. P-aSyn (S129) area fraction

was also quantified both within and outside neuronal masks (NeuN). Scans of the lumbar spinal cord were analyzed in QuPath (v. 0.5.1) and p-aSyn (S129) immunopositivity was computed using a pixel classifier on the DAB channel [6]. The data were normalized to the area of the region of interest (ROI) covering the ventral horn.

**Mouse Neuroanatomical Topography.** Panoramic views of digital slide scans were mapped onto Mouse Brain Atlas (Paxinos and Franklin's *The Mouse Brain in Stereotaxic Coordinates*, Elsevier Publishing, 4th Edition)- [27]. Information about neuroanatomical tracts and nuclei in mouse CNS was primarily derived from *The Mouse Nervous System* (Elsevier Publishing, 1st Edition)- [67].

**Statistics.** The data were statistically analyzed in Graphpad Prism software version 8, and the final graphs were prepared in Graphpad or Microsoft Excel. Statistical significance in datasets was calculated following the guidelines from relevant literature, as indicated in the figure legends. P values were set at: \* $p < 0.05$ , \*\* $p < 0.01$ , \*\*\* $p < 0.001$ , \*\*\*\* $p < 0.0001$ .

## Results

In this study, we aimed to refine an experimental paradigm of in vivo aSyn aggregation for studying the significance of prodromal aSyn pathology in GRN, particularly in the context of sensorimotor phenotypes relevant to PD. Lewy-related aSyn pathology affecting the GRN and nearby nuclei of the reticular formation in PD has been reported previously, using silver staining methods and/or immunodetection of aSyn using antibodies/anti-sera [8, 9, 58]. In order to assess the aggregation state of aSyn

in GRN, we performed IHC on post-mortem sections of medulla oblongata obtained from cases with clinically diagnosed parkinsonism (Table S1). For this purpose, we assessed the phosphorylation of aSyn on the serine residue S129 (p-aSyn, S129), which is one of the most widely used biochemical marker of aSyn pathology [1, 31, 60]. Our data corroborate the findings from pioneer studies, such that we observed significant accumulation of p-aSyn (S129) in the GRN of PD cases compared to the controls (Fig. 1A–B; antibody, EP1536Y).

To evaluate the consequences of aSyn aggregation in GRN in the rodent brain, we performed stereotaxic delivery of murine aSyn PFF into the pontine GRN of adult (12–14 weeks old) transgenic M83 mice, expressing the aggregation prone human mutant A53T aSyn [29]. This approach (i.e. delivery of exogenous PFF as seeding agents) for promoting de novo aSyn aggregation has been reproducibly used for studying the effects of aSyn-induced proteopathic stress in the nervous system, in both transgenic models and in wild type rodents [4, 14, 15, 24, 44, 56, 64]. Accordingly, we designed an experimental protocol in which we incorporated longitudinal assessment of select sensorimotor behaviors in heterozygous M83<sup>+/-</sup> mice, following PFF-mediated induction of aSyn aggregation in brain, with GRN as the initial nidus (Fig. 2A). Our main cohort consisted of heterozygous M83<sup>+/-</sup> mice injected with PFF aSyn (n=18; 9 males and 9 females), while monomeric aSyn and PBS vehicle injection were used as controls (n=5/group; 3 males, 2 females in each group). Using p-aSyn (S129) as a surrogate marker of cellular aSyn pathology [1, 31, 60], we also

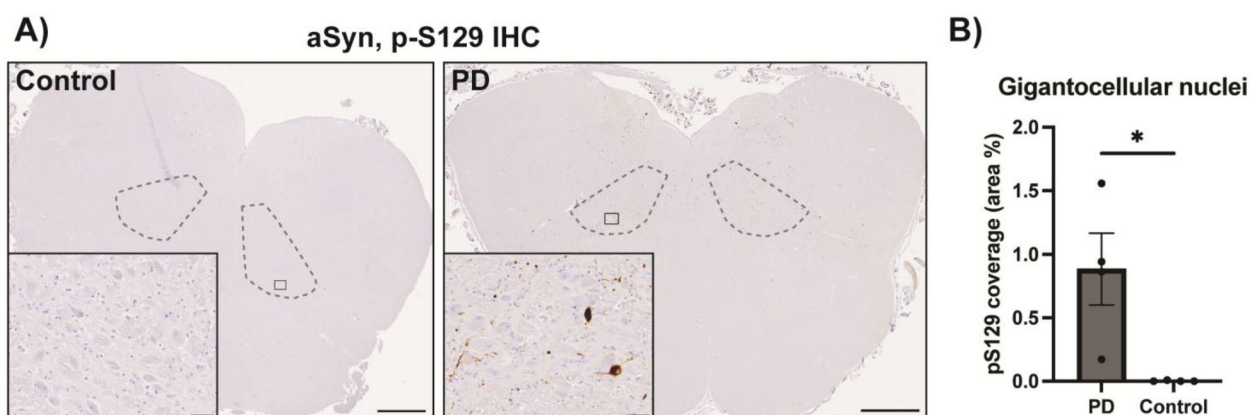


**Fig. 1** Immunostaining of phospho-alpha synuclein (p-aSyn, S129) in post-mortem human brain sections. **A** Representative images showing p-aSyn (S129) immunostaining in the transverse sections of medulla oblongata from controls and PD cases, with the gigantocellular nuclei (GRN) outlined by the dashed grey lines. Insets show high magnification images from the panoramic view, reflecting prominent Lewy pathology in PD and visible lack of staining in the controls. Scale bar = 2 mm (insets = 50  $\mu$ m). Primary antibody in Fig. 1A: p-aSyn (S129)- abcam EP1536Y. **B** Quantification shows that PD cases contain significantly more pS129-positive Lewy pathology than controls ( $p = 0.0286$ ). Graph displays mean  $\pm$  SEM of area % covered by p-aSyn S129 staining. Groups were compared with a Mann–Whitney test, as they did not pass the normality (Shapiro–Wilk) test. \* $p < 0.05$ , n = 4 per group

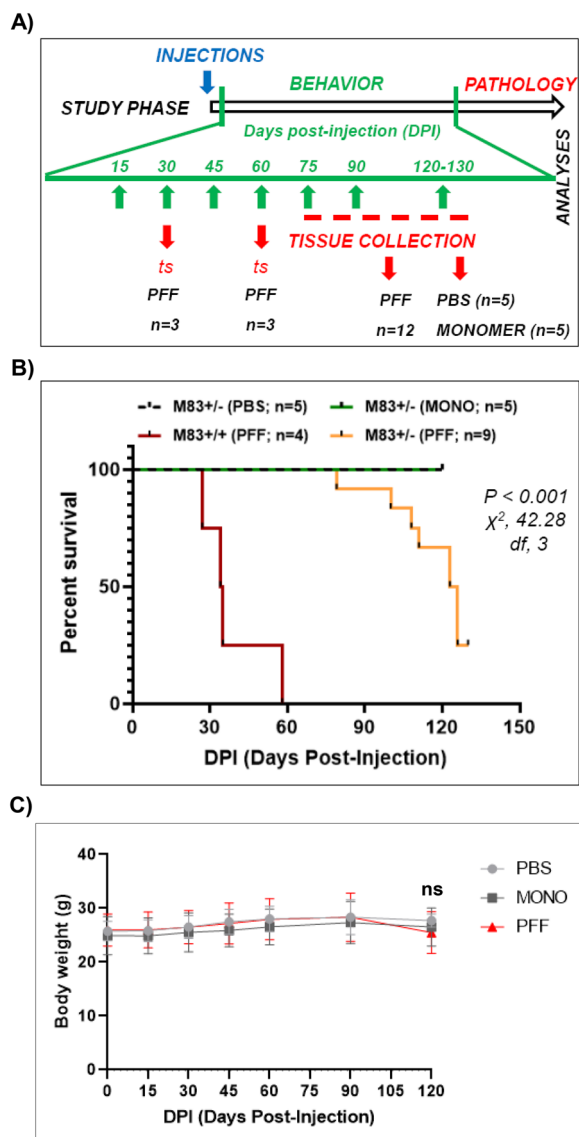


**Fig. 2** Overview of the study design in cohorts of heterozygous M83<sup>+/-</sup> mice. **A** In cohorts of transgenic M83<sup>+/-</sup> mice (12–14 weeks of age), phosphate buffered saline (PBS) vehicle (n = 5), monomeric (non-aggregated) aSyn (n = 5) or pre-formed fibrillar (PFF) aSyn (n = 18) were stereotactically delivered bilaterally in the pontine GRN/Gi. Post-recovery, the mice were periodically assessed over time in tests of sensorimotor behaviors (green arrows, median interval between measurements: 15 days, unless indicated otherwise in the figure legends). Timed tissue collection was performed from the PFF-injected cohort after sacrifice at 30 and 60 days post-injection (DPI) (n = 3/time-point), or in the event of a humane endpoint (period is highlighted by the dashed red line). The PBS and monomer cohorts were euthanized at the termination of the study (Between DPI-120 and DPI-130). **B** Kaplan–Meier plot showing survival of transgenic M83<sup>+/-</sup> mice injected with PBS, monomeric aSyn or PFF aSyn bilaterally in the pontine GRN/Gi. The survival analyses do not include mice from the M83<sup>+/-</sup> PFF aSyn cohort terminated at DPI-30 and DPI-60 (timed-sacrifice, mentioned in A). The median time to moribund state for the heterozygous M83<sup>+/-</sup> was 124.5 days post-injection (9 out of 12 animals reached a terminal stage by DPI-129; the 3 remaining animals were euthanized at DPI-130 and not included/censored in the survival analyses). A small cohort of homozygous M83<sup>+/+</sup> mice (n = 4) was also studied for comparison, in which the median time to a moribund state was 34.5 days. The PBS and monomeric injected mice M83<sup>+/-</sup> remained comparatively asymptomatic in gross motor performance (i.e. no foot-drop, paralysis or significant weight loss) over the duration of the experiment. Statistics in Fig. 2B: Log-rank Mantel-cox test (M83<sup>+/-</sup> cohorts: PBS, n = 5; monomeric aSyn, n = 5; PFF aSyn, n = 12 and M83<sup>+/+</sup> cohort: n = 4; \*\*\*\*p < 0.0001;  $\chi^2, 42.28$ ;  $df, 3$ ). **C** Line graph showing the body weight measurements of the cohorts of heterozygous M83<sup>+/-</sup> mice over the duration of the study up to DPI-120. Statistics in Fig. 2C: Two-Way ANOVA with Geisser-Greenhouse correction (M83<sup>+/-</sup> cohorts: PBS, n = 5; monomeric aSyn, n = 5; PFF aSyn, n = 9–18;  $\chi^2, 189.4$ ;  $df, 1$ ; Error bars, Mean  $\pm$  SD; ns = not significant)

studied the induction of aSyn aggregation in GRN and its propagation into additional brain regions over time.

Here, we show that PFF-mediated induction of multifocal aSyn aggregate pathology in GRN and distinct nuclei of subcortical motor system in the brains of transgenic M83 mice led to the emergence of phenotypes reflecting altered patterns of spontaneous activity and progressive deterioration of motor performance. In brief, 9 out of the 12 PFF-injected heterozygous M83<sup>+/-</sup> mice reached a terminal stage within 129 days post-injection (DPI-129), with median time to a moribund state of 124.5 days (Fig. 2B). Among the animals which reached a terminal stage for euthanasia, 5 were males (median, 111 days) and 4 were females (median, 126 days); albeit,

due to the small sample size, these differences were not significant. These animals started to exhibit signs of unilateral foot-drop and/or bouts of prolonged inactivity near the terminal stage ( $\geq$  DPI-108). In comparison, the control M83<sup>+/-</sup> cohorts (PBS and monomeric aSyn) remained asymptomatic in gross appearance (i.e. no foot-drop, freezing or significant weight loss) over the duration of the experiment. The median body weight (in grams) difference in the heterozygous M83<sup>+/-</sup> cohorts between DPI-60 and the time of sacrifice beyond DPI-90 was: PBS, -1.3 g (n = 5), monomeric aSyn, -1.5 g (n = 5) and PFF aSyn, -1.3 g (n = 11)- Fig. 2C Prior to initiating the study in heterozygous M83<sup>+/-</sup> (Fig. 2A), we performed a pilot study in cohorts of homozygous M83<sup>+/+</sup> mice (n = 4; 12–16 weeks old), in which PFF aSyn delivery was associated with a highly unfavorable outcome with median time to a moribund state of 34.5 days (Fig. 2B). Albeit, the pilot study (using M83<sup>+/+</sup> mice) lacked appropriate controls, and a detailed behavioral characterization was not performed. Nevertheless, these observations are in congruence with previous reports that PFF aSyn

delivery in transgenic M83 mice is associated with progressive motor impairment and reduced survival, with significantly earlier onset in the homozygous mice compared with the heterozygous animals [24, 56, 59].

### Direct PFF aSyn delivery in the GRN leads to an early-onset phenotype characterized by progressive decline in spontaneous activity and decreased locomotion in M83<sup>+/-</sup> mice

In order to assess the effects of aSyn aggregation in GRN on spontaneous activity and locomotion in M83<sup>+/-</sup> mice, we employed non-invasive 24-h monitoring using DVC- digitally ventilated cages [51]. For this purpose, we tracked the animals' activity (DVC locomotion index, see Methods) over a longitudinal period, starting from DPI-36 to DPI-90. Our results show a progressive decline in the spontaneous locomotion of PFF aSyn-injected M83<sup>+/-</sup> mice (n=12, in 4 cages), which could be clearly distinguished from the controls by DPI-60 (Fig. 3A; compare PBS and monomeric aSyn; n=5/in 2 cages/group). Moreover, evaluation of daily rhythms and home cage activity during light/dark periods revealed that the PFF-injected M83<sup>+/-</sup> mice were significantly less active during the dark period (night time, active time for rodents), compared to the controls (PBS and monomeric aSyn; Fig. 3B, C; complete data on daily rhythms are presented in Fig. S1).

In parallel, we also assessed the locomotion pattern and exploratory behavior of the mice in open-field arena at DPI-60, DPI-90 and DPI-120. Intriguingly, while the findings in DVC suggest a progressive reduction in activity by the PFF aSyn-injected cohort as early as DPI-60, all the experimental groups showed a similar pattern of activity in the open-field arena at DPI-60 and DPI-90 (Fig. S2A–B). However, at the advanced stage of the study (DPI-120), distinct locomotion patterns between the groups could be distinguished (Fig. 3D–G; S2C). Near termination, the PFF and monomeric aSyn-injected mice moved shorter distances (Fig. 3E), were slower (Fig. 3F), and exhibited

more frequent freezing episodes compared to the PBS cohort. Intriguingly, we also observed differences in entries to the periphery or center of the arena between the monomeric aSyn and PFF aSyn injected animals (Fig. S2B–C). A video montage of the open-field behavior is presented in the supplementary files accessible on the figshare repository (Table S2): VIDEO 1–5 (M83<sup>+/-</sup>) and VIDEO 18 (M83<sup>+/+</sup>) - see Data availability.

### PFF aSyn-injected M83<sup>+/-</sup> mice exhibit progressive defects in fine control of posture and balance

The experimental cohorts of M83<sup>+/-</sup> mice were also subjected to longitudinal assessment of motor coordination and balance using a battery of standard tests [2, 18, 37, 38]. During these assessments, PFF aSyn-injected M83<sup>+/-</sup> mice exhibited progressive deterioration of performance in the balancing beam test (Fig. 4A–C). These deficits were observed as early as DPI-45 on the narrow beam (diameter: 8 mm), such that the animals took longer time to traverse, experienced frequent slips of the hindpaws and had overall slower speed of movement, compared to the controls (Fig. 4A). Strikingly, the performance of all cohorts was relatively comparable on the wider beam (diameter: 16 cm) until DPI-90 (Fig. 4B), suggesting relatively intact postural reflexes and lack of gross motor weakness. The latter is further corroborated by the findings from the grip strength test (Fig. S2D), which ruled out major defects in motor strength and the ability to grab and hold surfaces. In the balance beam test, we also observed freezing of movement in the PFF aSyn-injected M83<sup>+/-</sup> cohort, with the mice hesitating to initiate the traversal and adopt a hunched posture (Fig. 4C). Near the terminal stage (DPI-120), slower movement and frequent hindpaw slips were eventually observed on the wider beam as well (Fig. 4B). Thus, these data (Fig. 4A–C) indicate a progressive nature of the deficits in fine control of postural adaptations in the PFF aSyn-injected M83<sup>+/-</sup> mice. A video montage of the performance in balance

(See figure on next page.)

**Fig. 3** Spontaneous activity and locomotion in cohorts of heterozygous M83<sup>+/-</sup> mice. **A–C** Non-invasive monitoring of spontaneous activity by cohorts of M83<sup>+/-</sup> mice in digitally ventilated cages (DVC) over a longitudinal period up to 56 days post-injection (DPI), starting at DPI-36. The line chart (in 3A) represents the cumulative locomotion index (x-axis, days), which is represented for light and dark periods (in 3B, x-axis showing time in minutes) and heatmaps (in 3C, x-axis showing time in hours over 24-h period each day, y-axis showing days with DPI-36 as the starting point on top). Also see line charts in S1A–D, displaying daily locomotion index for each day, including light and dark periods. Statistics in Fig. 3A: One-Way ANOVA followed by Dunn's multiple column comparisons (PBS, n=5 housed in 2 cages; monomeric aSyn, n=5 housed in 2 cages and PFF aSyn, n=12 housed in 4 cages; \**p*<0.05; Error bars, Mean ± SD). Only significant differences are highlighted. **D–G** Measurements of spontaneous activity by cohorts of M83<sup>+/-</sup> mice in the open-field arena recorded over 10 min (ANY-maze, see Material and Methods) and representative tracking plots (in 3D) at the indicated time points (Days post-injection: DPI-60, DPI-90 and DPI-120). Bar graphs with individual points represent quantitative measurements of the overall distance travelled (in 3E), mean speed (in 3F) and time freezing (in 3G). Statistics in Fig. 3E–G: One-Way ANOVA followed by Tukey's multiple column comparisons (PBS, n=5; monomeric aSyn, n=5 and PFF aSyn, n=9; \**p*<0.05, \*\**p*<0.01; Error bars, Mean ± SD). Only significant differences are highlighted. Also see Fig. S2A–B for data from the open field test at time-points DPI-60 and DPI-90

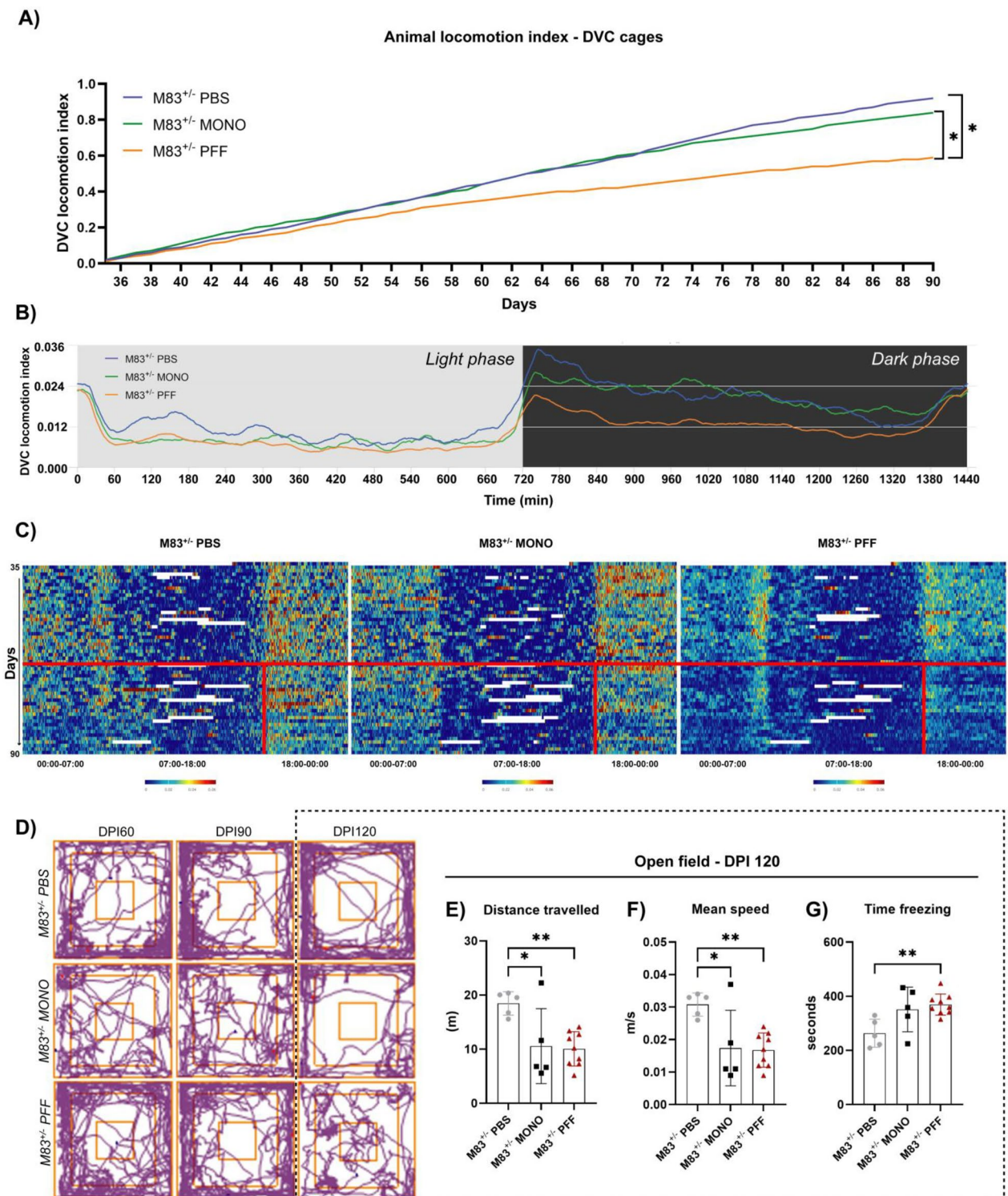


**Fig. 3** (See legend on previous page.)

beam test is presented in the supplementary files accessible on the figshare repository (Table S2): VIDEO 6–9 (M83<sup>+/-</sup>) and VIDEO 19 (M83<sup>+/+</sup>)- see Data availability.

#### Impaired performance in complex sensorimotor tasks and defective response to nociceptive stimuli is a late-stage phenotype in the PFF aSyn-injected M83<sup>+/-</sup> mice

We also subjected the experimental cohorts of M83<sup>+/-</sup> mice to tests requiring more complex sensorimotor skills and motor coordination. Among these, the pole test and the accelerating rotarod are commonly employed methods for phenotype assessment in models of basal ganglia disorders, including aSyn overexpressing rodents [2, 18]. In the pole test, the performance of experimental cohorts was overall comparable during the early stage of the study (DPI-60) (Fig. 4D, top panel). In contrast, significant differences between PFF aSyn-injected M83<sup>+/-</sup> mice and controls were seen near the terminal stage (DPI-120; Fig. 4D, bottom panel). At DPI-120, the PFF aSyn cohort exhibited increased latency in the turning response; however, the increased latency in descending and more time spent on the pole is due to assigning the cut-off test values to 3 out of 6 mice (see Methods). A video montage of the performance in the pole test is presented in the supplementary files accessible on the figshare repository (Table S2): VIDEO 10–13 (M83<sup>+/-</sup>)- see Data availability. The severity of movement incoordination was further substantiated by the findings from the rotarod test, in which the performance of PFF aSyn cohort at DPI ≥ 60 was significantly impaired in comparison with the controls (Fig. 4E; latency to fall, speed at fall).

Taken in conjunction, these findings indicate that gross defects in movement coordination following PFF aSyn delivery in the GRN are features defining the advanced stages of motor disability. This notion is further supported by assessments in the footprint test (gait stance)

and additional tasks requiring sensorimotor coordination (hindlimb clasp and response to nociceptive stimuli-see below). In the footprint test, we did not observe significant alterations in stride length, step width and base of support measurement between the cohorts (Fig. S3B–C) However, there were signs of uncoordinated gait at the pre-terminal stage (1–2 days before euthanasia, DPI ≥ 108) in 4 PFF aSyn-injected mice, reflected by the changes in step alternation during locomotion (Fig. S3B, S3D; compare instances indicated by green arrows and red arrows, reflecting coordinated gait or gait incoordination respectively). In one female (euthanized DPI-123), signs of imminent unilateral foot-drop could also be seen (Fig. S3B).

Another prominent phenotype in the M83 mice, reported as a harbinger of motor collapse in the presence of established brainstem aSyn pathology, is moderate-to-severe degree of hindlimb clasp [20, 24, 28]. This sensorimotor reflex is reliant upon an intact postural motor coordination, and is also impaired in models of basal ganglia, cerebellar or motor neuron dysfunction [41]. In the early stage (DPI-60), we observed a normal response (score 0) or mild degree (score 1) of hindlimb clasp in the controls, and 50% of the PFF aSyn-injected mice (Fig. 4F). Around DPI-120, ~30% animals in the PFF aSyn cohort progressed to moderate-severe degree of clasp (Fig. 4F; scores 2–3), suggesting potential dysfunction in pathways mediating this reflex response. A video montage of the hindlimb clasp test is presented in the supplementary files accessible on the figshare repository (Table S2): VIDEO 14–17 (M83<sup>+/-</sup>) and VIDEO 20 (M83<sup>+/+</sup>)- see Data availability.

Lastly, a previous study suggested that PFF aSyn delivery, using intramuscular injections, impaired nociception and mechanical allodynia in the M83<sup>+/-</sup> mice [23]. Therefore, we also assessed sensorimotor reflexes of nociception/allodynia using thermal or tactile stimuli (Hot plate

(See figure on next page.)

**Fig. 4** Measurements of sensorimotor behaviors in cohorts of heterozygous M83<sup>+/-</sup> mice. **A–B** Assessment of motor coordination of M83<sup>+/-</sup> cohorts (injected with PBS, monomeric aSyn or PFF aSyn) in the balancing beam test over a longitudinal period (shown on x-axis as DPI, days post-injection). The line graphs show the traversal time (seconds), number of slips and speed (m/s) on 8 mm wide beam (in 4A) and 16 mm wide beam (in 4B). **C** Representative images showing postural adaptations and performance on 8 mm beam by PBS or PFF-injected M83<sup>+/-</sup> mice. **D** Bar graphs depicting performance of M83<sup>+/-</sup> cohorts (injected with PBS, monomeric aSyn or PFF aSyn) in the pole test with individual points representing the quantitative measurement of the turning time, traversal time and total time on pole at DPI-60 and DPI-120 (DPI, days post-injection). **E** Assessment of motor coordination of M83<sup>+/-</sup> cohorts (injected with PBS, monomeric aSyn or PFF aSyn) in the rotarod test over a longitudinal period (shown on x-axis as DPI, days post-injection). The line graphs depict the quantitative measures of the latency to fall (time, in seconds) and speed at fall (rotations per minute, RPM). **F** Postural reflex assessment in modified tail-suspension test with bar graphs depicting hindlimb clasp by cohorts of M83<sup>+/-</sup> mice (injected with PBS, monomeric aSyn or PFF aSyn) at DPI-60 and DPI-120 (DPI, days post-injection). **G–H** Assessment of thermal nociception (hot plate, in 4G) and mechanical allodynia (von Frey, in 4H) in cohorts of M83<sup>+/-</sup> mice (injected with PBS, monomeric aSyn or PFF aSyn). Statistics in Fig. 4A–H: One-Way ANOVA followed by Tukey's multiple column comparisons (PBS, n = 5; monomeric aSyn, n = 5 and PFF aSyn, n = 6–9; \**p* < 0.05, \*\**p* < 0.01; Error bars, Mean ± SD). Black asterisks (all panels) represent significant differences between PBS and PFF aSyn-injected cohorts, while the grey asterisks (in 4A, 4E and 4G) indicate significant differences between monomeric aSyn and PFF aSyn-injected cohorts. Only significant differences are highlighted

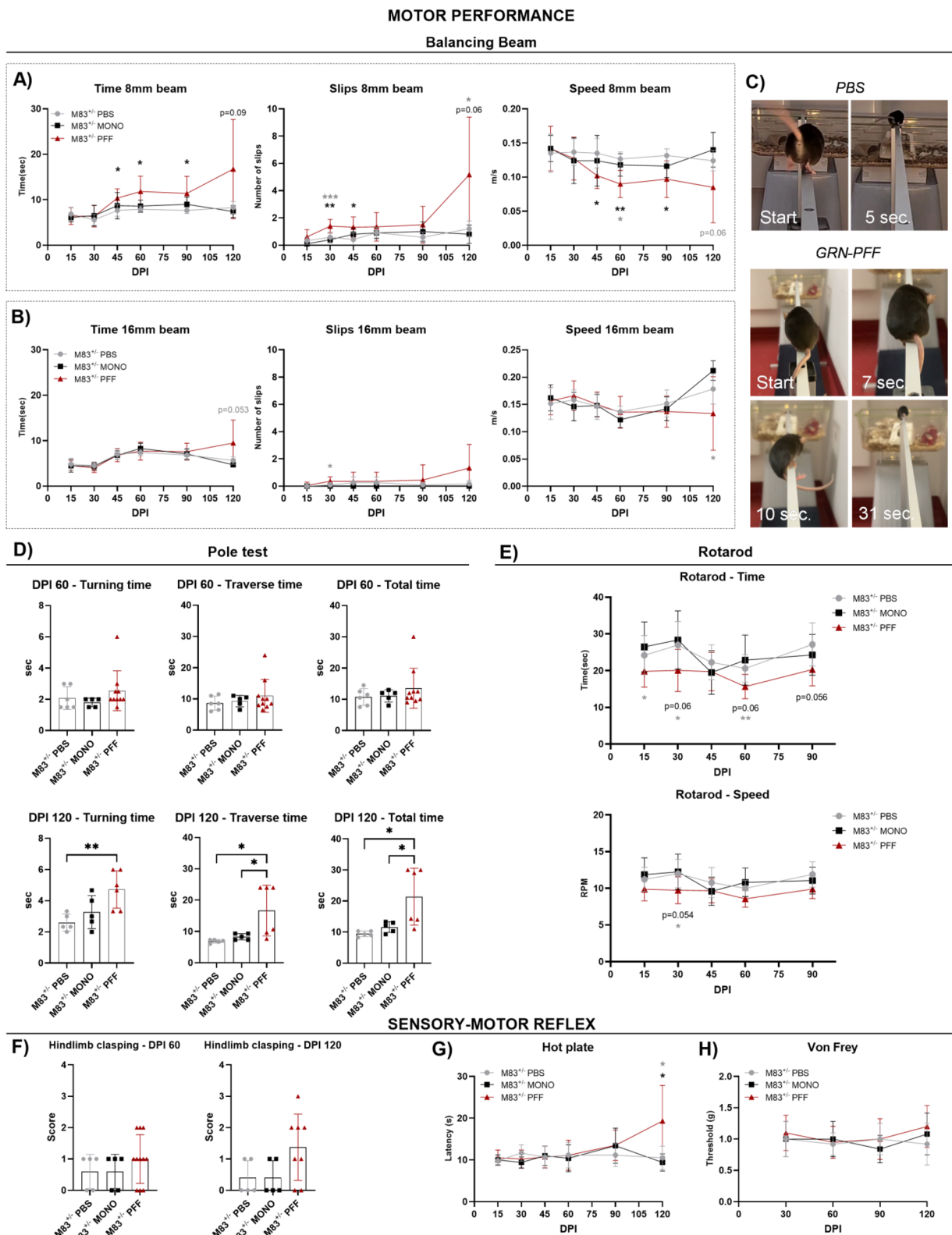


**Fig. 4** (See legend on previous page.)

and Von Frey filaments, respectively). In these tests, we observed that all experimental cohorts responded similarly throughout the study (i.e. exhibited an intact nociceptive response, in Fig. 4G–H). Although, we observed a relatively increased latency in the Hot plate in the PFF aSyn-injected cohort around DPI-120 (Fig. 4G), given the defects in movement coordination at this stage, we are unable to conclude if this reflects general motor weakness or a sensory defect in nociception.

#### **PFF aSyn delivery induces de novo aSyn aggregation in the GRN with spatiotemporal progression in brainstem**

In addition to the behavioral characterization, we wanted to contextualize the nature of neuronal aSyn pathology that potentially underlies the early and late phenotypes in movement coordination in M83<sup>+/-</sup> mice, following PFF aSyn delivery in the GRN (Figs. 3 and 4). Accordingly, we assessed the emergence and spatiotemporal progression of aSyn pathology in select brain regions (Fig. S4). Our analyses were guided by previous studies in M83 mice, showing substantial p-aSyn (S129) accumulation (spontaneous age-related, or PFF-induced) in the nuclei of the reticular formation including the GRN, midbrain PAG and vestibular nuclei (VN) [4, 24, 29, 56, 59]. Moreover, a mild-to-moderate degree of aSyn aggregation has also been detected in the deep cerebellar nuclei (DCN), red nucleus (RN) and motor cortex (M1/M2). Notably, pathological involvement of the substantia nigra (SN), striatum (caudatoputamen, CPu) and parts of thalamus is rarely observed in the M83 line [4, 24, 29, 56, 59].

By IF analyses (antibody: EP1536Y), we detected a sparse degree of p-aSyn (S129) accumulation in the GRN of PBS-injected mice at DPI-120 (Figs. 5A, 6B), likely due to spontaneous aSyn aggregation in the ageing transgenic M83<sup>+/-</sup> mice. In contrast, substantially more p-aSyn (S129) was detected in the GRN of the monomeric aSyn-injected cohort at DPI-120, in both neuronal cell bodies and in the surrounding neuropil (Figs. 5B and 6B). In the PFF aSyn injected mice, localized p-aSyn (S129) was detected within the GRN and adjacent pontine reticular formation as early as DPI-30 (Figs. 5C and 6A–B, S7B), and appeared to predominantly affect the neuropil (i.e. based on minimal overlap with neuronal nuclei marker, NeuN; Fig. S7A). Outside the GRN, we did not detect appreciable degree of p-aSyn (S129) accumulation at this early stage (Fig. 6A, S5A–E, S7B; regions shown in S5: VN, DCN, RN, PAG, and subthalamic nucleus- STh; also see Fig. S8A–D, lumbar spinal cord- ventral horn). By DPI-60, there was further increase in p-aSyn (S129) within GRN, characterized by a mixed pattern of accumulation in neuronal perikarya and surrounding neuropil (Figs. 5C and 6A–B, S7A–B). Among the other regions examined, p-aSyn (S129) was detected in the VN, and to

a lesser extent in the DCN, RN, PAG and STh at this stage (Fig. 6A, S5A–E, S7B). Moreover, sparse degree of p-aSyn (S129) was conspicuous in the ventral horn and intermediate grey matter of the lumbar spinal cord (Fig. S8B, D). The progressive nature of PFF aSyn-induced pathology was further corroborated by the analyses at terminal stage (DPI ≥ 108), which revealed significantly increased detection of p-aSyn (S129) not only in the GRN (Figs. 5C and 6A–B, S7B) but also in additional brain regions. Among the latter, nuclei within pons, cerebellum and midbrain showed a higher degree of cellular p-aSyn (S129) accumulation, while STh and some regions in thalamus/hypothalamus were weakly immunopositive (Fig. 6A, S5A–E, S6A, S7B). Similarly, there was significant increase in the p-aSyn (S129) immunopositivity in the lumbar spinal cord of PFF aSyn cohort at the terminal stage (DPI ≥ 108), compared to the DPI-30 and DPI-60 cohorts (Fig. S8A–D). Lastly, in line with the previous reports, there was visible lack of p-aSyn (S129) accumulation in M1/M2, CPu and SN (Fig. S6A).

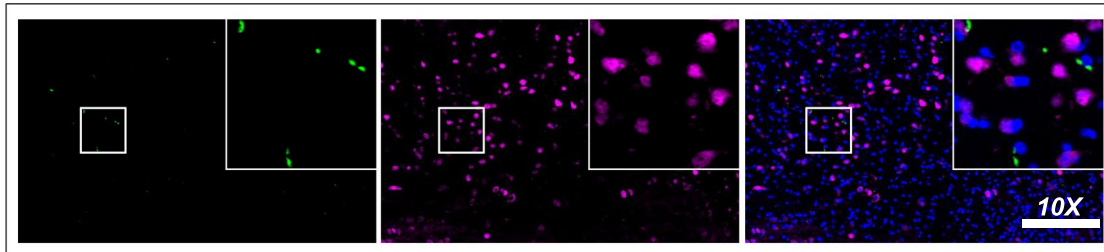
#### **PFF aSyn-induced aSyn aggregation in GRN of M83<sup>+/-</sup> mice is associated with neuroinflammation**

To further characterize the cellular aSyn pathology, we performed dual IF detection of p-aSyn (S129) with p62 protein (Sequestosome 1, a marker of intracellular protein aggregates and autophagy), or markers of inflammatory gliosis in the PFF aSyn-injected cohort. For this purpose, we restricted our analyses to GRN (initiation site in pons), PAG (a propagation site in midbrain) and M1/M2 (motor cortex, with minimal aSyn aggregation) in the terminal stage animals (DPI ≥ 108). As expected, p-aSyn (S129) aggregation within the GRN and PAG was associated with substantial p62 accumulation, reflected by IF co-detection of the two markers (Fig. S6B; compare M1/M2). In parallel, we also probed reactive astrogliosis and microglial infiltration, which have been reported as neuropathological features in the brains of M83 mice with advanced aSyn pathology [56, 59]. In the disease affected regions (GRN and PAG), we detected substantial expression of markers reflecting astroglia proliferation (GFAP, in Fig. S6C and S7C), and infiltration by phagocytic microglia (CD68, in Fig. S6D and S7D). In addition, we assessed the degree of neuronal loss in the GRN, as a potential underlying factor for the observed sensorimotor phenotypes in the PFF aSyn-injected cohort. Our analyses suggest a slight (albeit, non-significant) decrease in the total number of neurons in the GRN and adjacent part of the pontine reticular formation (Fig. 6C).

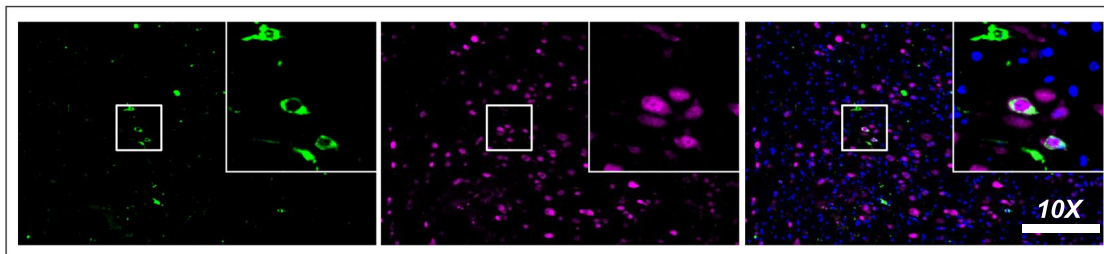
In addition to the detailed quantitative studies in heterozygous M83<sup>+/-</sup> cohorts presented above, we also examined p-aSyn (S129) accumulation in select brain regions of terminal stage homozygous M83<sup>+/+</sup> mice, following

## p-aSyn (S129), NeuN, DAPI in pontine GRN

## A) PBS (DPI-120)



## B) Monomeric aSyn (DPI-120)



## C) PFF aSyn (DPI-30 to terminal DPI ≥ 108)

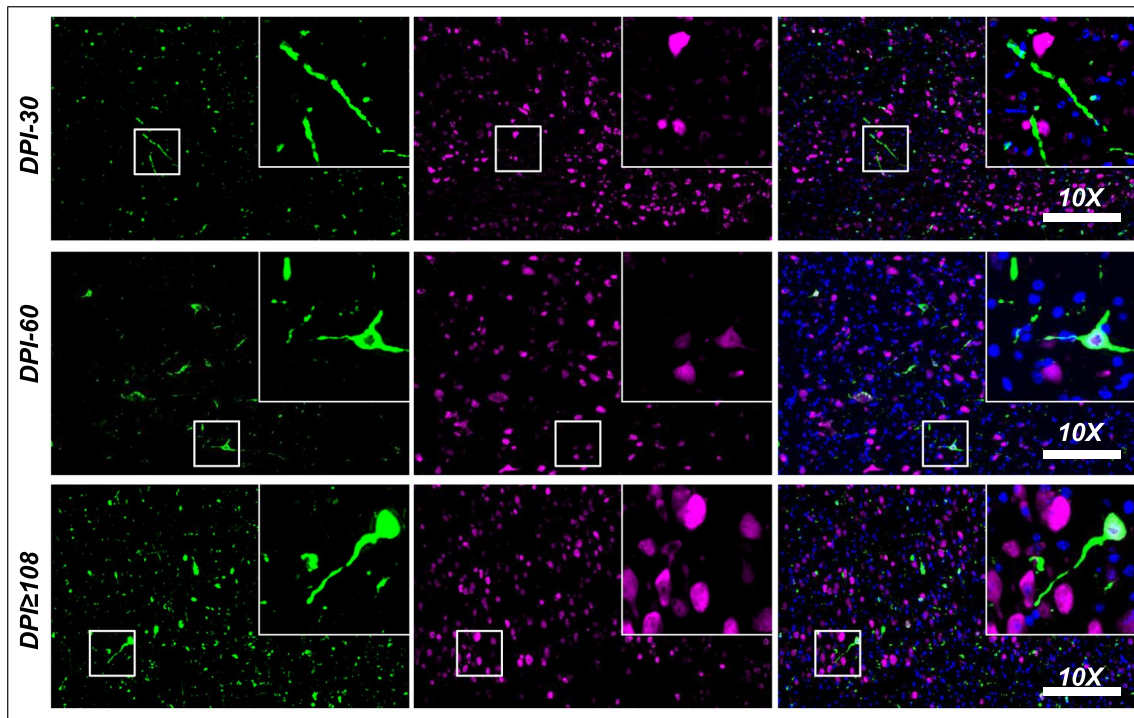


**Fig. 5** Dual immunofluorescence detection of phosphorylated alpha-synuclein (p-aSyn, S129) and neuronal nuclei (NeuN) in the GRN of M83<sup>+/+</sup> mice. **A–C** Representative low magnification (10X) images showing p-aSyn (S129) and neuronal nuclei (NeuN) immunofluorescence detection in the GRN/Gi of PBS (in 5A), monomeric aSyn (in 5B) and PFF aSyn (in 5C) injected M83<sup>+/+</sup> mice at indicated time-points (DPI, days post-injection). The insets show 63X magnified views of the GRN/Gi, highlighted by the white-bordered square in the 10X views (scale bar = 200 μm). Notice the neuritic and cellular aSyn pathology in monomeric aSyn-injected cohort (DPI-120, in 5B) and the PFF aSyn-injected cohort, which increases over time in the latter (DPI-30 to terminal stage DPI ≥ 108; also see Fig. 6B and S7A). A sparse degree of spontaneous aSyn pathology was also seen in the PBS-injected cohort (in 5A, DPI-120, age 7–8 months). Also see Supplementary Figures S5 (additional brain regions with p-aSyn, S129 positivity), S6–7 (markers of inflammatory gliosis) and S9 (p-aSyn S129 detection in the terminal-stage homozygous M83<sup>+/+</sup> mice, ≥ DPI-34). Primary antibodies in Fig. 5A–C: p-aSyn (S129)- abcam EP1536Y and NeuN- EMD Millipore A60

aSyn PFF delivery in the GRN (pilot study, Fig. 2B). While we have not performed detailed quantitative assessments, IF and IHC (DAB chromogen) suggested a similar pattern of regional p-aSyn (S129) distribution, such that the GRN and the nearby VN (in pons) and PAG (in midbrain) were among the most conspicuously affected regions (Fig. S9A–D). Moreover, the motor cortex (M1/M2) was largely devoid of p-aSyn (S129), as suggested by a sparse IF signal (Fig. S9E). Lastly, we aimed to rule out any bias in p-aSyn (S129) detection, which could potentially emanate from reliance on a single antibody (EP1536Y) used in the main analyses (Figs. 5 and 6, S5–S7). To this end, we employed a different polyclonal antibody (rabbit, D1R1R), and assessed p-aSyn (S129) immunostaining in the GRN of the terminal stage heterozygous M83<sup>+/-</sup> mice. By IF and IHC (DAB), both antibodies detected characteristic pattern of cellular p-aSyn (S129) immunostaining in the GRN, i.e. in neuronal perikarya and neuropil (Fig. S9A–B). Taken together, these analyses are compelling indicators of the pathological nature of p-aSyn (S129) accumulation in the brains of M83 mice, following PFF aSyn delivery in the GRN.

## Discussion

Progressive movement disability, in the form of difficulty in movement initiation (bradykinesia) and impaired postural reflexes (shuffling gait, difficulty in turning) is among the cardinal features of clinical parkinsonism. It is also recognized that pathological aSyn accumulation affecting distinct extra-nigral loci in the nervous system may precede the onset of clinical symptoms by several years, and depending on the initial site of aggregation, may dictate the course of disease progression [7, 12, 34, 36, 39, 48, 57]. Historically, the significance of extra-nigral brainstem aSyn pathology- to a large extent- has been investigated in the context of non-motor symptoms [10, 22, 37, 38, 49, 65]. Hence, experimental models of

extra-nigral brainstem aSyn pathology in the context of PD motor symptomatology are few and far between.

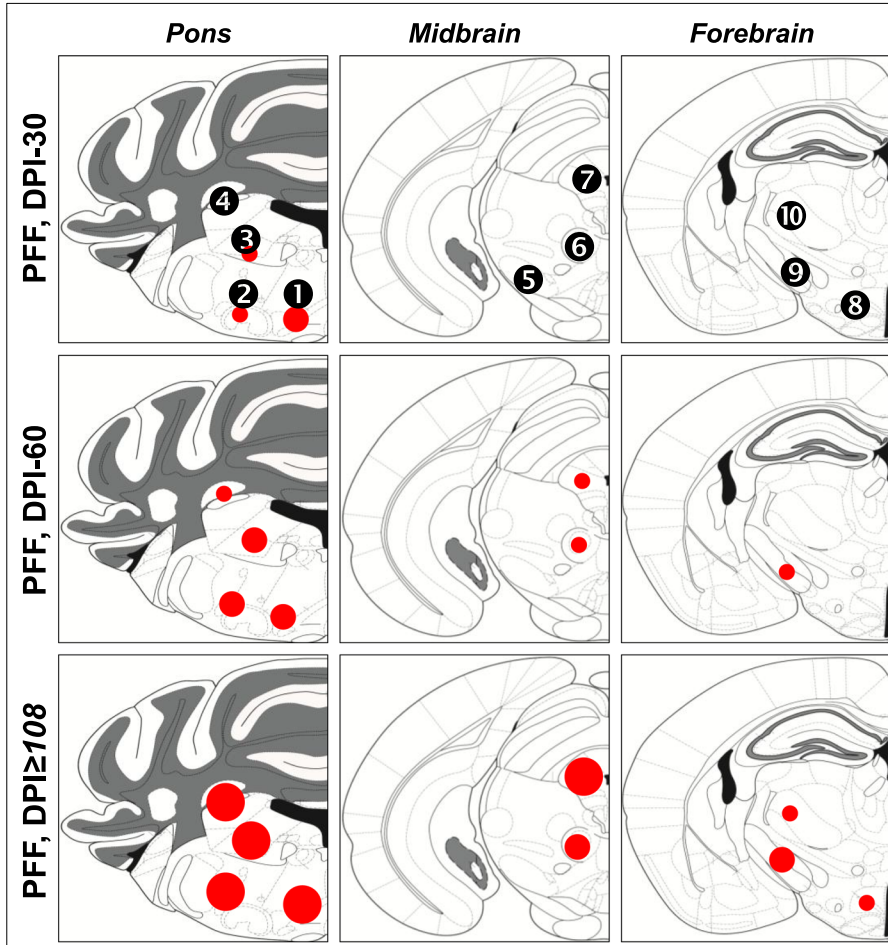
In this study, we investigated the significance of pathological aSyn aggregation in neuronal populations of the GRN in relation to features of movement disability in PD. Our data show that the initial phase of multi-focal aSyn pathology affecting the GRN and distinct nuclei of subcortical motor system (vestibular nuclei, cerebellar nuclei, red nucleus, subthalamic nucleus; Figs. 5C and 6A, B, S7B) in brains of heterozygous M83<sup>+/-</sup> mice was associated with progressive reduction in spontaneous locomotion (Fig. 3A, B, DVC) and concomitant defects in the fine control of postural reflexes (Fig. 4A–C, narrow beam). However, gross defects in locomotion patterns (Fig. 3D–G, open field) and signs of incoordination in complex sensorimotor tasks (Fig. 4D–F) emerged at a later stage, when widespread aSyn pathology and neuroinflammation were detected (Fig. S5–S7). Collectively, the spatiotemporal progression of cellular aSyn pathology and emergent sensorimotor phenotypes warrant further refining this experimental paradigm (discussed below), towards establishing the pathogenic significance of aSyn aggregation in the GRN.

Nevertheless, there are some key limitations that preclude major conclusions from the study presented above. The most obvious limitation is the small sample size and lack of detailed analyses for the controls at earlier time points (DPI-30 and DPI-60), especially monomeric aSyn injected animals. Close to the termination of the study (DPI-120), these animals also started to exhibit slight decline in the spontaneous activity (Fig. 3A–C) and altered patterns of locomotion in the open-field (Fig. 3D–G), in association with localized aSyn pathology in the GRN (Fig. 5B and 6B). Future studies could exploit this relatively slower aggregation paradigm and yield better insights into the natural history of motor phenotypes in the context of progression of aSyn pathology in this (GRN synucleinopathy) model. Another major limitation

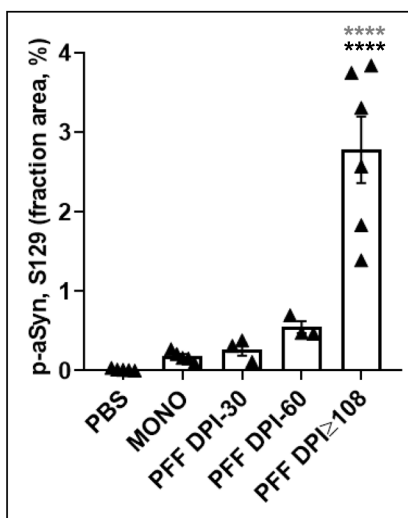
(See figure on next page.)

**Fig. 6** Composite schematic depiction of phosphorylated alpha-synuclein (p-aSyn, S129) immunofluorescence detection in the brains of M83<sup>+/-</sup> mice. **A** Average p-aSyn (S129) fluorescence signal (percentage of area) in the regions is highlighted by colored circles as follows: small circle (0.05–0.2%), medium circle (0.2–1%) and large circle (1–5%). Also see Supplementary Figure S4 for the low magnification (2X) panoramic views annotating select brain regions and S7B. Regions shown in 6A: (view in S4, Pons) ① gigantocellular nuclei (GRN), ② pontine reticular nuclei (Rt), ③ vestibular nuclei; ④ deep cerebellar nuclei; (view in S4, Midbrain) ⑤ substantia nigra, ⑥ red nucleus, ⑦ periaqueductal grey matter; (view in S4, Thalamus) ⑧ medial and lateral hypothalamus, ⑨ subthalamic nucleus, ⑩ ventromedial and ventrolateral thalamic nuclei. **B** Quantitative estimates of p-aSyn S129 immunopositivity (immunofluorescence signal intensity from two serial sections) in the GRN/Gi in cohorts of M83<sup>+/-</sup> mice, expressed as percentage of the area (total average area/image: 625,000  $\mu\text{m}^2$ ) in 10X views (see Fig. 5A–C). **C** Quantitative estimates of the total number of neurons (NeuN immunofluorescence) in of GRN/Gi from cohorts of M83<sup>+/-</sup> mice. Statistics in Fig. 6B–C: One-Way ANOVA followed by Tukey's multiple column comparisons (PBS, n = 5; monomeric aSyn, n = 5; PFF aSyn DPI-30 and DPI-60, n = 3 and PFF aSyn DPI  $\geq$  108, n = 5; \*\*\*\* $p < 0.0001$ ; Error bars, Mean  $\pm$  SD). (In Fig. 6B) Black asterisks represent significant differences between PBS and PFF aSyn-injected cohorts, while the grey asterisks indicate significant differences between monomeric aSyn and PFF aSyn-injected cohorts. Only significant differences are highlighted (Fig. 6B–C)

**A) p-aSyn, S129**



**B) p-aSyn, S129 (GRN)**



**C) NeuN (GRN)**

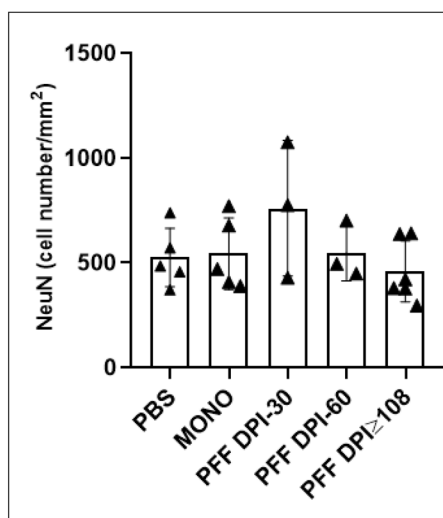


**Fig. 6** (See legend on previous page.)

of the study is that the observations have been made in transgenic M83 mice (overexpressing the aggregation prone, human mutant A53T aSyn), with an aggressive approach for inducing aSyn pathology (i.e. PFF aSyn delivery in the GRN). It is well established that naive M83 mice (i.e. without exogenous PFF aSyn injections) also exhibit age-related decline in locomotion, impaired performance in rotarod and a severe moribund phenotype near the terminal stage (lack of grooming, freezing, foot-drop and paralysis) [29, 56]. However, it is noteworthy that the phenotypes reported in naive M83 mice appear at much later ages than those observed in our study: i.e. 8–12 months in homozygous M83<sup>+/+</sup> and 20–24 months in heterozygous M83<sup>+/-</sup> mice [29, 56].

It has also been reported that the onset and progression of the motor phenotypes in M83 mice are significantly exacerbated by the exogenous delivery of PFF aSyn by peripheral routes, which results in initial aSyn pathology in spinal cord and subsequently across the neuraxis [3, 4, 56, 59]. In other words, the movement disability in M83 mice following peripheral PFF delivery in these prior studies is not attributed to aSyn pathology in a distinct brain region(s), but largely considered to emanate from the loss of spinal motor neurons [56, 59]. In the present study, our observations suggest that the progressive reduction in the locomotor activity (Fig. 3A–C, DVC) and postural instability (Figs. 3A–C, 4A–C) in the PFF aSyn-injected cohort emerge in association with multi-focal aSyn pathology beyond the GRN, affecting the vestibular nuclei, cerebellar nuclei, red nucleus and the subthalamic nucleus (Figs. 5C, 6A–B, S7B), and to a lesser extent the lumbar spinal cord (Fig. S8B–D). Therefore, from this pilot study, we are not able to conclusively establish that the observed phenotype is solely the result of aSyn aggregate pathology in the GRN.

Therefore, a refined approach to validate this model (of aSyn aggregation in GRN) is needed. It is important that the behavioral phenotypes (bradykinesia and postural instability) are assessed in an experimental paradigm with localized and relatively slower propagation of aSyn aggregation in GRN, instead of the aggressive PFF aSyn-based approach used in this proof-of-concept study. In other words, it is plausible that the damage inflicted by PFF injection is not restricted to the nerve cell bodies in the GRN only but also affects the nerve terminals of the projection regions and nearby vestibular nuclei, which in turn represent a confounding factor with regards to interpreting the nature of motor disability in the model. Hence, for achieving localized aSyn aggregation in the GRN, future studies could exploit the direct delivery of monomeric aSyn (e.g., comparing wild type and mutant A53T aSyn) or ectopic expression of human aSyn transgene in the GRN using viral vectors [37, 38]. In this

context, the injection of monomeric aSyn is considered a control experiment; however, our data show that given sufficient time, this can also trigger de novo aSyn aggregation at the injection site (Fig. 5B, S7B; compare to PBS) and affect patterns of locomotion (Fig. 3A–G, DPI-120). These observations are reminiscent of a recent study which reported that intrastriatal injections of comparable amounts (2  $\mu$ l of 5  $\mu$ g/ $\mu$ l) of monomeric aSyn in wild type mice stimulates local microglial immune response, and defects in motor performance as early as 1 month post-injection [25].

The AAV-based approach is also advantageous, since it could help dissect dysfunction in distinct neuronal sub-populations in the GRN, which potentially underlie the movement disability in this model. Technically, this is feasible in genetically modified rodents in which human transgene(s) expression can be achieved in target neuronal populations by the stereotaxic delivery of engineered viral vectors, as demonstrated for cre-recombinase expressing dopaminergic neurons in vivo [5]. Thus, we consider that the validation of this model of neurodegenerative aggregate pathology in the GRN, and further refinements to this experimental paradigm hold promise for novel translational approaches in PD and related disorders. To illustrate, recent studies show that chemogenetic activation of *Chx10* neurons in the GRN of rodents helps restore turning defects induced by striatal dopamine deficiency following 6-OHDA administration [17].

In a larger context, several animal models based on aSyn overexpression (transgenic or through viral vector delivery) have been studied, and differ with regards to their fidelity in recapitulating features of movement disability in PD ((Reviewed elsewhere- [37, 38]). These studies show that the phenotypes in each model are also affected by the promoter driving aSyn expression, which in turn potentially dictates the spatiotemporal features of aSyn aggregation in distinct neuronal populations [21, 29, 54]. For instance, transgenic models with aSyn expression (A53T or E46K) under the control of prion promoter (*Prnp*) exhibit severe motor phenotypes, most likely due to age-related decline in spinal motor neurons as mentioned above [29, 56, 59]. In comparison, the transgenic lines based on the thymus cell antigen 1 (*Thy1*) promoter driven aSyn overexpression exhibit age-related progression of motor features, as well as altered circadian rhythm and sleep [40, 55]. Hence, it would be interesting to assess the effects of direct PFF aSyn delivery in the GRN of *Thy1-SNCA* strains in relation to motor and non-motor phenotypes. Intriguingly, we found that the pattern of spontaneous locomotion in PFF aSyn injected M83<sup>+/-</sup> mice was significantly affected during the nocturnal phase (Fig. 3B–C). It is unclear whether this phenotype of reduced nocturnal activity potentially

reflects altered sleep–wake cycles and circadian rhythm disturbances, and is worth further investigations. Especially, given that subdivisions of the GRN and adjacent nuclei of reticular formation have been implicated in the REM sleep behavior disorder (RBD)- [46, 50], this could present an area for the follow-up studies evaluating the non-motor phenotypes (which were not analyzed in the current study). Lastly, there are isolated reports in the published literature showing that monomeric aSyn injection into the GRN of wild type mice leads to progressive decline in dopamine concentration and tyrosine hydroxylase mRNA expression in the striatum; however, behavioral outcomes were not assessed or reported [35]. Thus, characterizing the neurochemical aspects within the GRN and its associated subcortical motor circuitry in this model could further facilitate the identification of neural substrate(s) underlying the features of movement disability in this model.

## Conclusion

In conclusion, we consider that our study highlights a crucial role of prodromal aSyn pathology in the GRN in features of movement disability in PD. We also anticipate that our data will stimulate novel hypotheses in model development for studying the significance of neuronal dysfunction in the motor circuitry of the GRN in relation to phenotypes relevant to PD.

## Supplementary Information

The online version contains supplementary material available at <https://doi.org/10.1186/s40478-025-01948-7>.

Additional file 1.

## Acknowledgements

The authors would like to thank the animal caretaker staff at the Department of Biomedicine- AU (DK) for assistance, and J.G.J.M. (John) Bol at UMC Amsterdam (NL) for histopathology on the human tissue sections.

## Author contributions

VT, SAF, MRR and AJ designed research; VT, SAF, NMJ, DMG, MR, MWH, IF, HG and AJ performed research; SAF, NMJ, OAA and EDR performed data analyses; WDjvdB provided immunostaining data on human post-mortem tissue and contributed to discussion; PHJ, PB, JRN, CBV and NVDB contributed with infrastructural and personnel support, data evaluation and discussion; VT, SAF and AJ wrote the manuscript. All the authors read and approved the current version of the manuscript.

## Funding

This work was supported by funding to AJ in the form of a Michael J. Fox Foundation grant (grant# MJFF-021498). HG and PHJ was supported by Lundbeck Foundation grants R383-2022–180, R248-2016–2518 for Danish Research Institute of Translational Neuroscience-DANDRITE, Nordic-EMBL Partnership for Molecular Medicine.

## Data availability

All the data generated and analyzed during this study are included in the main manuscript and the associated supplementary files. A video montage of

select behaviors (Table S2) is accessible on the figshare repository: <https://doi.org/https://doi.org/10.6084/m9.figshare.26936968>.

## Declarations

### Ethics approval and consent to participate

Post-mortem brain tissue from subjects with clinical parkinsonism and neurologically normal controls were acquired from the Netherlands Brain Bank (NBB; Amsterdam, The Netherlands, <http://brainbank.nl>). Donors or their next of kin signed informed consent for brain autopsy, the use of brain tissue and the use of medical records for research purposes. The brain donor program of the NBB and NABCA is approved by the local medical ethics committee of the VUmc, Amsterdam (approva I# NBB 2009.148). For a detailed description of cases and cohorts, see Reference [66]. Ethical approval for the transgenic M83 mouse colonies (housing, breeding) and the experimental procedures was obtained by the relevant authorities of Denmark (Dyreforsøgstilsynet) approval # 2022–15-0201–01294 issued to CBV, co-author.

### Consent for publication

Not applicable. The manuscript does not contain an individual person's data in any form.

### Competing interests

The authors declare no competing interests.

### Author details

<sup>1</sup>Department of Clinical Medicine, Aarhus University, Palle Juul-Jensens Boulevard 35, 8200 Aarhus, Denmark. <sup>2</sup>Department of Biomedicine, Aarhus University, Høegh-Guldbergs Gade 10, 8000 Aarhus, Denmark. <sup>3</sup>Department of Biomedicine, Danish Research Institute of Translational Neuroscience (DANDRITE), Aarhus University, Ole Worms Allé 3, 8000 Aarhus C, Denmark. <sup>4</sup>Core Center for Molecular Morphology, Department of Clinical Medicine, Aarhus University, Palle Juul-Jensens Boulevard 35, 8200 Aarhus, Denmark. <sup>5</sup>Department of Pathology, Aarhus University Hospital, Palle Juul-Jensens Boulevard 35, 8200 Aarhus, Denmark. <sup>6</sup>Department of Anatomy and Neurosciences, Amsterdam Neuroscience, VU University Medical Center Amsterdam, De Boelelaan 1117, 1081 HV Amsterdam, The Netherlands. <sup>7</sup>Department of Molecular Biology and Genetics, Aarhus University, Universitetsbyen 81, 8000 Aarhus, Denmark.

Received: 4 October 2024 Accepted: 5 February 2025

Published online: 17 February 2025

## References

- Anderson JP, Walker DE, Goldstein JM, de Laat R, Banducci K, Caccavello RJ et al (2006) Phosphorylation of Ser-129 is the dominant pathological modification of alpha-synuclein in familial and sporadic Lewy body disease. *J Biol Chem* 281:29739–29752. <https://doi.org/10.1074/jbc.M600933200>
- Aniszewska A, Bergstrom J, Ingelsson M, Ekmark-Lewen S (2022) Modeling Parkinson's disease-related symptoms in alpha-synuclein overexpressing mice. *Brain Behav* 12:e2628. <https://doi.org/10.1002/brb3.2628>
- Ayers JI, Brooks MM, Rutherford NJ, Howard JK, Sorrentino ZA, Riffe CJ et al (2017) Robust central nervous system pathology in transgenic mice following peripheral injection of alpha-synuclein fibrils. *J Virol*. <https://doi.org/10.1128/JVI.02095-16>
- Ayers JI, Riffe CJ, Sorrentino ZA, Diamond J, Fagerli E, Brooks M et al (2018) Localized induction of wild-type and mutant alpha-synuclein aggregation reveals propagation along neuroanatomical tracts. *J Virol*. <https://doi.org/10.1128/JVI.00586-18>
- Backman CM, Malik N, Zhang Y, Shan L, Grinberg A, Hoffer BJ et al (2006) Characterization of a mouse strain expressing Cre recombinase from the 3' untranslated region of the dopamine transporter locus. *Genesis* 44:383–390. <https://doi.org/10.1002/dvg.20228>
- Bankhead P, Loughrey MB, Fernandez JA, Dombrowski Y, McArt DG, Dunne PD et al (2017) QuPath: open source software for digital pathology image analysis. *Sci Rep* 7:16878. <https://doi.org/10.1038/s41598-017-17204-5>

7. Borghammer P (2021) The alpha-synuclein origin and connectome model (SOC Model) of Parkinson's disease: explaining motor asymmetry, non-motor phenotypes, and cognitive decline. *J Parkinsons Dis* 11:455–474. <https://doi.org/10.3233/JPD-202481>
8. Braak H, Del Tredici K, Rub U, de Vos RA, Jansen Steur EN, Braak E (2003) Staging of brain pathology related to sporadic Parkinson's disease. *Neurobiol Aging* 24:197–211
9. Braak H, Rub U, Sandmann-Keil D, Gai WP, de Vos RA, Jansen Steur EN et al (2000) Parkinson's disease: affection of brain stem nuclei controlling pre-motor and motor neurons of the somatomotor system. *Acta Neuropathol* 99:489–495. <https://doi.org/10.1007/s004010051150>
10. Butkovich LM, Houser MC, Chalermpananupap T, Porter-Stransky KA, Iannitelli AF, Boles JS et al (2020) Transgenic mice expressing human alpha-synuclein in noradrenergic neurons develop locus ceruleus pathology and nonmotor features of parkinson's disease. *J Neurosci* 40:7559–7576. <https://doi.org/10.1523/JNEUROSCI.1468-19.2020>
11. Carter RJ, Lione LA, Humby T, Mangiarini L, Mahal A, Bates GP et al (1999) Characterization of progressive motor deficits in mice transgenic for the human Huntington's disease mutation. *J Neurosci* 19:3248–3257. <https://doi.org/10.1523/JNEUROSCI.19-08-03248.1999>
12. Cheng HC, Ulane CM, Burke RE (2010) Clinical progression in Parkinson disease and the neurobiology of axons. *Ann Neurol* 67:715–725. <https://doi.org/10.1002/ana.21995>
13. Chopek JW, Zhang Y, Brownstone RM (2021) Intrinsic brainstem circuits comprised of Chx10-expressing neurons contribute to reticulospinal output in mice. *J Neurophysiol* 126:1978–1990. <https://doi.org/10.1152/jn.00322.2021>
14. Chu WT, DeSimone JC, Riffe CJ, Liu H, Chakrabarty P, Giasson BI et al (2020) alpha-synuclein induces progressive changes in brain microstructure and sensory-evoked brain function that precedes locomotor decline. *J Neurosci* 40:6649–6659. <https://doi.org/10.1523/JNEUROSCI.0189-20.2020>
15. Chung HK, Ho HA, Perez-Acuna D, Lee SJ (2019) Modeling alpha-synuclein propagation with preformed fibril injections. *J Mov Disord* 12:139–151. <https://doi.org/10.14802/jmd.19046>
16. Cregg JM, Leiras R, Montalant A, Wanken P, Wickersham IR, Kiehn O (2020) Brainstem neurons that command mammalian locomotor asymmetries. *Nat Neurosci* 23:730–740. <https://doi.org/10.1038/s41593-020-0633-7>
17. Cregg JM, Sidhu SK, Leiras R, Kiehn O (2024) Basal ganglia-spinal cord pathway that commands locomotor gait asymmetries in mice. *Nat Neurosci* 27:716–727. <https://doi.org/10.1038/s41593-024-01569-8>
18. Delenclos M, Farooqi AH, Yue M, Kurti A, Castanedes-Casey M, Rousseau L et al (2017) Neonatal AAV delivery of alpha-synuclein induces pathology in the adult mouse brain. *Acta Neuropathol Commun* 5:51. <https://doi.org/10.1186/s40478-017-0455-3>
19. Dickson DW (2018) Neuropathology of Parkinson disease. *Parkinsonism Relat Disord* 46(Suppl 1):S30–S33. <https://doi.org/10.1016/j.parkreidis.2017.07.033>
20. Earls RH, Menees KB, Chung J, Gutekunst CA, Lee HJ, Hazim MG et al (2020) NK cells clear alpha-synuclein and the depletion of NK cells exacerbates synuclein pathology in a mouse model of alpha-synucleinopathy. *Proc Natl Acad Sci U S A* 117:1762–1771. <https://doi.org/10.1073/pnas.1909110117>
21. Emmer KL, Waxman EA, Covy JP, Giasson BI (2011) E46K human alpha-synuclein transgenic mice develop Lewy-like and tau pathology associated with age-dependent, detrimental motor impairment. *J Biol Chem* 286:35104–35118. <https://doi.org/10.1074/jbc.M111.247965>
22. Farrell KF, Krishnamachari S, Villanueva E, Lou H, Alerte TN, Peet E et al (2014) Non-motor parkinsonian pathology in aging A53T alpha-synuclein mice is associated with progressive synucleinopathy and altered enzymatic function. *J Neurochem* 128:536–546. <https://doi.org/10.1111/jnc.12481>
23. Ferreira N, Goncalves NP, Jan A, Jensen NM, van der Laan A, Mohseni S et al (2021) Trans-synaptic spreading of alpha-synuclein pathology through sensory afferents leads to sensory nerve degeneration and neuropathic pain. *Acta Neuropathol Commun* 9:31. <https://doi.org/10.1186/s40478-021-01131-8>
24. Ferreira N, Richner M, van der Laan A, Bergholdt Jul Christiansen I, Vaegter CB, Nyengaard JR et al (2021) Prodromal neuroinvasion of pathological alpha-synuclein in brainstem reticular nuclei and white matter lesions in a model of alpha-synucleinopathy. *Brain Commun* 3:fcab104. <https://doi.org/10.1093/braincomms/fcab104>
25. Ferreira SA, Li C, Klæstrup IH, Vitic Z, Rasmussen RK, Kirkegaard A et al (2023) Sex-dimorphic neuroprotective effect of CD163 in an alpha-synuclein mouse model of Parkinson's disease. *npj Parkinson's Disease* 9:164. <https://doi.org/10.1038/s41531-023-00606-w>
26. Fitzgerald M (2005) The development of nociceptive circuits. *Nat Rev Neurosci* 6:507–520. <https://doi.org/10.1038/nrn1701>
27. Franklin KBJ, Paxinos G (2013) Paxinos and Franklin's The mouse brain in stereotaxic coordinates. Academic Press, an imprint of Elsevier, City
28. Gallagher E, Hou C, Zhu Y, Hsieh CJ, Lee H, Li S et al (2024) Positron emission tomography with [(18)F]ROStrace reveals progressive elevations in oxidative stress in a mouse model of alpha-synucleinopathy. *Int J Mol Sci*. <https://doi.org/10.3390/ijms25094943>
29. Giasson BI, Duda JE, Quinn SM, Zhang B, Trojanowski JQ, Lee VM (2002) Neuronal alpha-synucleinopathy with severe movement disorder in mice expressing A53T human alpha-synuclein. *Neuron* 34:521–533. [https://doi.org/10.1016/s0896-6273\(02\)00682-7](https://doi.org/10.1016/s0896-6273(02)00682-7)
30. Glajch KE, Fleming SM, Surmeier DJ, Osten P (2012) Sensorimotor assessment of the unilateral 6-hydroxydopamine mouse model of Parkinson's disease. *Behav Brain Res* 230:309–316. <https://doi.org/10.1016/j.bbr.2011.12.007>
31. Goedert M, Jakes R, Spillantini MG (2017) The synucleinopathies: twenty years on. *J Parkinsons Dis* 7:S51–S69. <https://doi.org/10.3233/JPD-179005>
32. Haines DE, Mihailoff GA (2018) Fundamental neuroscience for basic and clinical applications. Elsevier, City
33. Hoglinger GU, Adler CH, Berg D, Klein C, Outeiro TF, Poewe W et al (2024) A biological classification of Parkinson's disease: the SynNeurGe research diagnostic criteria. *Lancet Neurol* 23:191–204. [https://doi.org/10.1016/S1474-4422\(23\)00404-0](https://doi.org/10.1016/S1474-4422(23)00404-0)
34. Jellinger KA (2019) Is Braak staging valid for all types of Parkinson's disease? *J Neural Transm (Vienna)* 126:423–431. <https://doi.org/10.1007/s00702-018-1898-9>
35. Joniec-Maciejak I, Ciesielska A, Poniatowski LA, Wawer A, Szejder-Pacholek A, Wojnar E et al (2019) Effects of alpha-synuclein monomers administration in the gigantocellular reticular nucleus on neurotransmission in mouse model. *Neurochem Res* 44:968–977. <https://doi.org/10.1007/s11064-019-02732-5>
36. Kalia LV, Lang AE (2015) Parkinson's disease. *Lancet* 386:896–912
37. Konnova EA, Swanberg M (2018) Animal Models of Parkinson's Disease. In: Stoker TB, Greenland JC (eds) *Parkinson's Disease: Pathogenesis and Clinical Aspects*, City
38. Koprach JB, Kalia LV, Brotchie JM (2017) Animal models of alpha-synucleinopathy for Parkinson disease drug development. *Nat Rev Neurosci* 18:515–529. <https://doi.org/10.1038/nrn.2017.75>
39. Kordower JH, Olanow CW, Dodiya HB, Chu Y, Beach TG, Adler CH et al (2013) Disease duration and the integrity of the nigrostriatal system in Parkinson's disease. *Brain* 136:2419–2431. <https://doi.org/10.1093/brain/awt1192>
40. Kudo T, Loh DH, Truong D, Wu Y, Colwell CS (2011) Circadian dysfunction in a mouse model of Parkinson's disease. *Exp Neurol* 232:66–75. <https://doi.org/10.1016/j.expneurol.2011.08.003>
41. Lalonde R, Strazielle C (2011) Brain regions and genes affecting limb-clasping responses. *Brain Res Rev* 67:252–259. <https://doi.org/10.1016/j.brainresrev.2011.02.005>
42. Lemieux M, Bretzner F (2019) Glutamatergic neurons of the gigantocellular reticular nucleus shape locomotor pattern and rhythm in the freely behaving mouse. *PLoS Biol* 17:e2003880. <https://doi.org/10.1371/journal.pbio.2003880>
43. Liang H, Watson C, Paxinos G (2016) Terminations of reticulospinal fibers originating from the gigantocellular reticular formation in the mouse spinal cord. *Brain Struct Funct* 221:1623–1633. <https://doi.org/10.1007/s00429-015-0993-z>
44. Luk KC, Kehm VM, Zhang B, O'Brien P, Trojanowski JQ, Lee VM (2012) Intracerebral inoculation of pathological alpha-synuclein initiates a rapidly progressive neurodegenerative alpha-synucleinopathy in mice. *J Exp Med* 209:975–986. <https://doi.org/10.1084/jem.20112457>
45. Luong TN, Carlisle HJ, Southwell A, Patterson PH (2011) Assessment of motor balance and coordination in mice using the balance beam. *J Vis Exp*. <https://doi.org/10.3791/2376>

46. Luppi P-H, Malcey J, Chancel A, Duval B, Cabrera S, Fort P (2024) Neuronal network controlling REM sleep. *J Sleep Res*. <https://doi.org/10.1111/jsr.14266>
47. Martin GF, Vertes RP, Waltzer R (1985) Spinal projections of the gigantocellular reticular formation in the rat. evidence for projections from different areas to laminae I and II and lamina IX. *Exp Brain Res* 58:154–162. <https://doi.org/10.1007/BF00238963>
48. McCann H, Stevens CH, Cartwright H, Halliday GM (2014) alpha-Synucleinopathy phenotypes. *Parkinsonism Relat Disord* 20(Suppl 1):S62–67. [https://doi.org/10.1016/S1353-8020\(13\)70017-8](https://doi.org/10.1016/S1353-8020(13)70017-8)
49. Menozzi E, Macnaughtan J, Schapira AHV (2021) The gut-brain axis and Parkinson disease: clinical and pathogenetic relevance. *Ann Med* 53:611–625. <https://doi.org/10.1080/07853890.2021.1890330>
50. Nardone R, Golaszewski S, Höller Y, Christova M, Trinkka E, Brigo F (2013) Neurophysiological insights into the pathophysiology of REM sleep behavior disorders: a review. *Neurosci Res* 76:106–112. <https://doi.org/10.1016/j.neures.2013.03.009>
51. Piilgaard L, Rose L, Justinussen JL, Hviid CG, Lemcke R, Wellendorph P et al (2023) Non-invasive detection of narcolepsy type I phenotypical features and disease progression by continuous home-cage monitoring of activity in two mouse models: the HCRT-KO and DTA model. *Sleep*. <https://doi.org/10.1093/sleep/zsad144>
52. Poewe W, Seppi K, Tanner CM, Halliday GM, Brundin P, Volkman J et al (2017) Parkinson disease. *Nat Rev Dis Primers* 3:17013. <https://doi.org/10.1038/nrdp.2017.13>
53. Richner M, Bjerrum OJ, Nykjaer A, Vaegter CB (2011) The spared nerve injury (SNI) model of induced mechanical allodynia in mice. *J Vis Exp*. <https://doi.org/10.3791/3092>
54. Rockenstein E, Mallory M, Hashimoto M, Song D, Shults CW, Lang I et al (2002) Differential neuropathological alterations in transgenic mice expressing alpha-synuclein from the platelet-derived growth factor and Thy-1 promoters. *J Neurosci Res* 68:568–578. <https://doi.org/10.1002/jnr.10231>
55. Rothman SM, Griffioen KJ, Vranis N, Ladenheim B, Cong WN, Cadet JL et al (2013) Neuronal expression of familial Parkinson's disease A53T alpha-synuclein causes early motor impairment, reduced anxiety and potential sleep disturbances in mice. *J Parkinsons Dis* 3:215–229. <https://doi.org/10.3233/JPD-120130>
56. Sacino AN, Brooks M, Thomas MA, McKinney AB, Lee S, Regenhardt RW et al (2014) Intramuscular injection of alpha-synuclein induces CNS alpha-synuclein pathology and a rapid-onset motor phenotype in transgenic mice. *Proc Natl Acad Sci U S A* 111:10732–10737. <https://doi.org/10.1073/pnas.1321785111>
57. Schapira AHV, Chaudhuri KR, Jenner P (2017) Non-motor features of Parkinson disease. *Nat Rev Neurosci* 18:435–450. <https://doi.org/10.1038/nrn.2017.62>
58. Seidel K, Mahlke J, Siswanto S, Kruger R, Heinsen H, Auburger G et al (2015) The brainstem pathologies of Parkinson's disease and dementia with Lewy bodies. *Brain Pathol* 25:121–135. <https://doi.org/10.1111/bpa.12168>
59. Sorrentino ZA, Xia Y, Funk C, Riffe CJ, Rutherford NJ, Ceballos Diaz C et al (2018) Motor neuron loss and neuroinflammation in a model of alpha-synuclein-induced neurodegeneration. *Neurobiol Dis* 120:98–106. <https://doi.org/10.1016/j.nbd.2018.09.005>
60. Spillantini MG, Schmidt ML, Lee VM, Trojanowski JQ, Jakes R, Goedert M (1997) Alpha-synuclein in Lewy bodies. *Nature* 388:839–840. <https://doi.org/10.1038/42166>
61. Stringer C, Wang T, Michaelos M, Pachitariu M (2021) Cellpose: a generalist algorithm for cellular segmentation. *Nat Methods* 18:100–106. <https://doi.org/10.1038/s41592-020-01018-x>
62. Thomsen MB, Ferreira SA, Schacht AC, Jacobsen J, Simonsen M, Betzer C et al (2021) PET imaging reveals early and progressive dopaminergic deficits after intra-striatal injection of preformed alpha-synuclein fibrils in rats. *Neurobiol Dis* 149:105229. <https://doi.org/10.1016/j.nbd.2020.105229>
63. Turner PV, Pang DS, Lofgren JL (2019) A review of pain assessment methods in laboratory rodents. *Comp Med* 69:451–467. <https://doi.org/10.30802/AALAS-CM-19-000042>
64. Uchihara T, Giasson BI (2016) Propagation of alpha-synuclein pathology: hypotheses, discoveries, and yet unresolved questions from experimental and human brain studies. *Acta Neuropathol* 131:49–73. <https://doi.org/10.1007/s00401-015-1485-1>
65. Van Den Berge N, Ferreira N, Mikkelsen TW, Alstrup AKO, Tamguney G, Karlsson P et al (2021) Ageing promotes pathological alpha-synuclein propagation and autonomic dysfunction in wild-type rats. *Brain* 144:1853–1868. <https://doi.org/10.1093/brain/awab061>
66. van der Gaag BL, Deshayes NAC, Breve JJP, Bol J, Jonker AJ, Hoozemans JJM et al (2024) Distinct tau and alpha-synuclein molecular signatures in Alzheimer's disease with and without Lewy bodies and Parkinson's disease with dementia. *Acta Neuropathol* 147:14. <https://doi.org/10.1007/s00401-023-02657-y>
67. Watson C, Paxinos G, Puelles L (2012) The mouse nervous system. Elsevier Academic Press, City
68. Wilson-Poe AR, Pocius E, Herschbach M, Morgan MM (2013) The periaqueductal gray contributes to bidirectional enhancement of antinociception between morphine and cannabinoids. *Pharmacol Biochem Behav* 103:444–449. <https://doi.org/10.1016/j.pbb.2012.10.002>
69. Yerger J, Cougnoux AC, Abbott CB, Luke R, Clark TS, Cawley NX et al (2022) Phenotype assessment for neurodegenerative murine models with ataxia and application to Niemann-Pick disease, type C1. *Biol Open*. <https://doi.org/10.1242/bio.059052>

## Publisher's Note

Springer Nature remains neutral with regard to jurisdictional claims in published maps and institutional affiliations.